Weather Types and Rainfall over Senegal. Part I: Observational Analysis

Vincent Moron[1] , Andrew W. Robertson, M. Neil Ward, Ousmane NDiaye

International Research Institute for Climate and Society,

The Earth Institute at Columbia University

Palisades, New York

submitted to *Journal of Climate*

Manuscript : JCLI 1601

submitted : July 19, 2006

revised : April 12, 2007

[1] Corresponding author address : Vincent Moron, UFR des Sciences Géographiques et de l'Aménagement, Université d'Aix-Marseille and CEREGE, UMR-6635 CNRS (email : moron@cerege.fr).

Abstract

A *k*-means cluster analysis is used to summarize unfiltered daily atmospheric variability at regional-scale over the western Sahel and eastern tropical North Atlantic during the boreal summer season (July—September, JAS) 1961—1998. It employs zonal and meridional regional wind fields at 925, 700 and 200 hPa from the European Centre for Medium-Range Weather Forecast Reanalyses. An 8-cluster solution is shown to yield an integrated view of the complex regional circulation variability, without the need for explicit time filtering. Five of the weather types identified characterize mostly typical phases of westward moving wave disturbances, as African Easterly Waves –AEWs–, and persistent monsoon surges, while the three others describe mostly different stages of the seasonal cycle. Their temporal sequencing describes a systematic monsoonal evolution, together with considerable variability at sub-seasonal and inter-annual time scales.

Daily rainfall occurrence at 13 gauge stations in Senegal is found to be moderately well-conditioned by the 8 weather types, with positive rainfall anomalies usually associated with southerly wind anomalies at 925 hPa. Interannual variability of daily rainfall frequency is shown to depend substantially on the frequency of occurrence of weather types specific to the beginning and end of the JAS season, together with the number of persistent monsoon surges over the western Sahel. In contrast, year-to-year changes in the frequency of the weather types mostly associated with westward moving waves as AEWs are not found to influence seasonal frequency of occurrence of daily rainfall substantially.

The fraction of seasonal rainfall variability related to weather type frequency is found to have a strong relationship with tropical Pacific sea surface temperatures (SSTs): an El Niño (La Niña) event tends to be associated with a higher (lower) frequency of dry early and late JAS season weather types with enhanced trade winds over the western Sahel, together with lower (higher) prevalence of persistent monsoon surges. The component of seasonal rainfall variability *not* related to weather-type frequency is characterized by changes in rainfall probability within each weather type, especially those occurring in the core of the JAS

season; it exhibits a larger decadal component that is associated with an SST pattern previously identified with recent observed trends in Sahel rainfall.

1. Introduction

Many previous studies have investigated the inter-annual and longer term variability of seasonal mean rainfall in the Sahel region in general (i.e. Nicholson, 1979; Fontaine and Bigot, 1993; Moron, 1994; Rowell *et al.*, 1995; Ward, 1998) as well as for Senegal in particular (Camberlin and Diop, 1999, 2003). Folland *et al.* (1986) demonstrated the association between the changes in sea surface temperatures (SST) and Sahelian seasonal mean rainfall variability. Several of the above studies (Lamb, 1978; Hastenrath, 1984, 1990; Rowell *et al.*, 1995; Ward, 1998) identified a strong relationship between the inter-hemispheric gradient of SST and multi-decadal variability of Sahelian rainfall. The relationships between SST and Sahelian rainfall at inter-annual time scales are more complex and less stable (Janicot *et al.*, 1996; Ward, 1998). Wetter (drier) conditions in the Sahel are usually associated with cold (warm) El Niño Southern Oscillation (ENSO) events, anomalously cold (warm) SST anomalies (SSTAs) over the equatorial and southern Atlantic and the western Indian ocean and anomalously warm (cold) SSTAs over the northern tropical Atlantic. These empirical relationships have been largely confirmed by atmospheric General Circulation Models (AGCM) experiments with historical SSTs prescribed (Rowell *et al.*, 1995; Moron *et al.*, 1998, 2004; Giannini *et al.*, 2003; Paeth and Friederichs, 2004). Such experiments have been highly successful at simulating the multi-decadal variability of Sahelian rainfall (Giannini *et al.,* 2003), though relatively few models are successful at inter-annual time scales, especially during the post-1967 dry period (Sperber and Palmer, 1996; Moron *et al.*, 2003; Moron, 2005).

The above studies have focused almost exclusively on seasonal mean rainfall, while very little attention has been given to the inter-annual variability of sub-seasonal quantities such as the number of rainy days, length of dry/wet spells etc. Rainfall over West Africa during the summer monsoon is mainly associated with meso-scale convective systems, especially over the Sahel (D'Amato and Lebel, 1998; Laurent *et al.*, 1998; Lebel *et al.*, 2003). These are often, but not always, embedded within African Easterly Waves – AEWs– (Burpee, 1972) that arise from barotropic/baroclinic instability of the middle troposphere African Easterly jet (AEJ) extended W-E over most of the Sahel near 15°N. Nevertheless, the link between

convection (and rainfall) and easterly waves is far from linear and remains controversial (Thorncroft and Rowell, 1998; Diedhiou *et al.,* 1998, 1999, 2001; Grist, 2002; Gu and Adler, 2004; Gu *et al.*, 2004). Fink and Reiner (2003) argue that the strength of coupling between AEWs and meso-scale convective systems increases toward the West-African coast, consistent with the observed westward growth of wave amplitude. Taleb and Druyan (2003) indicated that > 70% of the seasonal rainfall at Dakar are accounted by 3-9 day variability of meridional wind at 700 hPa, consistent with 3-5 and 6-9 day AEW regimes (Dhiediou *et al.*, 1998, 1999, 2001). AEWs are not the only sub-seasonal modulator of the rainfall. Janicot and Sultan (2001) identified a westward propagating quasi-periodic signal with a period of about 15-40 days. This signal is associated with the meridional shift of the ITCZ (Sultan and Janicot, 2000) and the surges of the West-African monsoon (Louvet *et al.*, 2003). Even slower sub-seasonal components have also been identified (Sultan *et al.*, 2003; Matthews 2004). In summary, the sub-seasonal variability of rainfall in Sahel is composed of the interactions between inter-related processes with various time and space scales (Sultan *et al.*, 2003; Druyan *et al.*, 2006). It is little understood how these sub-seasonal processes are influenced by SST forcing.

Most of the studies cited above used band-pass filtered time series to analyze sub-seasonal variability and its relationship with local-to-regional rainfall within a specified frequency range. A different approach is pursued here, based on an objective clustering method (*k*-means) that is used to partition *unfiltered* daily atmospheric variability into different weather types. In the extra-tropics, such a clustering scheme is commonly used to define so-called "weather regimes" (Mo and Ghil, 1988; Molteni *et al.*, 1990). These weather regimes are usually interpreted as preferred states of a nonlinear dynamical system with a chaotic attractor (Ghil and Robertson, 2002). They are characterized by persistent large-scale flow patterns that appear repeatedly at fixed geographical locations and organize the behavior of synoptic-scale motions during several days or weeks (Michelangeli *et al.*, 1995; Robertson and Ghil, 1999). As the name implies, weather regimes affect local weather. The "episodic" approach to circulation variability, via cluster analysis, has been shown to be complementary to an "oscillatory" approach, via spectral analysis, both

conceptually (Ghil and Robertson, 2002) and in practice, the latter using for example a *k*-means analysis of Pacific-South American circulation variability (Robertson and Mechoso, 2003). Even in the case of a propagating wave, a cluster analysis may provide a useful coarse-grained discretization of the wave, with a "resolution" provided by the number of clusters chosen.

The goals of the present study are; (i) to propose an objective partitioning of the regional-scale atmospheric circulation variability over the western Sahel and eastern Tropical North Atlantic (0°-30°W, 5°-25°N), considering all time scales; and (ii) to analyze how these "weather types" affect local rainfall in Senegal. The use of these weather types in downscaling studies is illustrated in part II of this study (Moron *et al.*, 2007b, referred hereafter as Part II). Section 2 describes the daily station rainfall dataset together with the reanalysis atmospheric circulation data. The weather types are presented in section 3. A summary and conclusions are presented in section 4.

2. Datasets

a. Rainfall

The study uses a 13-station network (Fig. 1a) of daily rainfall observations over Senegal as in Moron *et al.* (2006, 2007a). This network includes the 10 main synoptic stations of the country and 3 non-synoptic stations (i.e. Diouloulou, Kounghel and Goudiry). The data used in this study covers the period from July, 1, 1961 to September 30, 1998 (JAS hereafter). The lack of available daily rainfall data after 1998 prevented the use of a longer period, but the analyzed time series includes parts of the predominantly wet and dry periods before and after 1968 (i.e. Nicholson, 1979 ; Moron, 1994). The dataset is complete although some of the data are doubtful. In particular, the three non-synoptic stations have significantly less wet days between 0 and 1 mm than the neighboring stations. The possible related bias in the frequency of occurrence of rainy days is eliminated by using a threshold of 1 mm for defining wet days (Moron *et al.*, 2007a).

Senegal is a flat Sahelian country neighboring the Tropical North Atlantic. As for the entire Sahel, the rainy season grows longer southward (Fig. 1b,c), associated with the latitudinal migration of the Inter-Tropical Convergence Zone (ITCZ). Daily rainfall occurrence frequency (days receiving > 1 mm) usually peaks between August 25 and September 5, north of 13.5°N (Fig. 1b). The seasonal cycle is flatter for the 4 southernmost stations (i.e. Ziguinchor, Diouloulou, Kolda and Kedougou) with almost no difference between July 20 and September 10 (Fig. 1b). The amplitude of the seasonal cycle is small for the mean daily rain amount on wet days with a peak around the end of August in the northern two-thirds of the country (Fig. 1c); it is also small in southern Senegal (i.e. higher rainfall amount from July 20 to September 10) associated with higher rainfall rates than in the north-central part of the country (Fig. 1c).

b. ERA-40

The ECMWF (European Centre for Medium-Range Weather Forecast) 40-year reanalysis project (ERA-40, Simmons and Gibson, 2000) data are used to describe variability of the atmospheric circulation. The data are available on a 2.5° x 2.5° grid every 6 hours from September 1, 1957 to August 31, 2002. The daily mean of the zonal and meridional components of the winds at 925, 700 and 200 hPa over the area (30°W-0°, 5°-25°N) from July 1, 1961 to September 30, 1998 are used in the following. Figure 2 displays the mean July-September climatology of the wind at 200 hPa (Fig. 2a) 700 hPa (Fig. 2b) and 925 hPa (Fig. 2c), as well as the mean seasonal cycle of these winds over Senegal (Fig. 2d,e,f). The low-level winds exhibit the classical low level monsoon flow with a convergence near 7°N over the Tropical Atlantic and shifted northward to near 20°N at 0°E, associated with the thermal low centered over the Sahara (Fig. 2c). The predominantly westerly flow over Senegal is strongest during late July and is replaced by northeasterlies in September (Fig. 2f). The main feature of the middle troposphere is the African Easterly jet (AEJ) with axis near 15°N (Fig. 2b); it is only weakly modulated by the seasonal cycle during the period in ERA-40, with a slight weakening after mid-July (Fig. 2e). The Tropical Easterly jet (TEJ) dominates the upper troposphere, with Senegal near its northern margin (Fig. 2a). Its axis is located south of the AEJ, and its seasonal cycle matches that at lower levels peaking around the

end of July (Fig. 2d), i.e. before the rainy peak of the JAS season (Fig. 1b,c). The mean upper-level winds become weak westerlies in late September (Fig. 2d). Note that the ERA-40 fields were linearly interpolated from the original 2.5 x 2.5 degree grid onto a T42 Gaussian grid for the following analyses, to facilitate the use of the ECHAM4.5 GCM simulations in Part II.

3. Weather types

a. Definition of the number of weather types

A standard *k*-means cluster analysis is applied to the 7 leading unstandardized principal components (PC) of both zonal and meridional components of the ERA-40 daily winds, accounting for 52% of their daily variance. Considering more PCs to retain a larger fraction of the variance, yields very similar weather types but slows the computations used in Part II. *K*-means is an iterative clustering procedure (Diday and Simon, 1976) that consists in partitioning the data into *k* clusters so as to minimize the sum of variance within-cluster. The first step concerns to choose the appropriate number of clusters. This is determined using two statistical scores : the classifiability index (Michelangeli *et al.*, 1995; Plaut and Simonnet, 2001) and the information criterion (Santos *et al.*, 2005).

The classifiability index (CI) measures the dependence of a partition into *k* clusters on the initial seeds. Here 100 partitions are performed in the subspace defined by the leading 7 PCs, for *k* varying from 2 to 10 using randomly chosen initial seeds. The similarity between two partitions is calculated in terms of the anomaly correlation coefficient between the cluster centroïds in the PC-space (Michelangeli *et al.*, 1995). For any cluster *i* of partition **P**, the cluster of partition **Q** with maximum anomaly correlation coefficient defines the cluster *j* that most resembles it. The minimum value of this distribution defines the CI for cluster *i* of partition **P**, *i.e.* the *worst-fitting* counterpart. When two partitions are identical, CI = 1 for all clusters. CI is computed for 100 partitions and averaged to give a CI for a number *k* of clusters. The best partition maximizes the CI averaged across the *k* clusters.

For reference, we define a first-order Markov process having the same covariance at lag 0 and 1 as the unstandardized leading 7 PCs of wind data, following Michelangeli *et al.* (1995) and Plaut and Simonnet (2001). This 7-dimensional noise model is used to generate 100 samples of the same length as the wind dataset and CI is calculated for each of them. The CI is shown on Fig. 3a as a function of the number of clusters, together with the two-sided 95% confidence bounds. The CI drops to a minimum at $k = 5$ and then increases to a plateau above 0.70 for $k = 8$ to 10; it emerges from the noise for $k = 3$, then from $k = 7$. The fact that CI is quite stable from $k = 7$ is further discussed below. The classifiability of any dataset is closely related to the reproducibility of clusters (Michelangeli *et al.*, 1995).

While the CI yields information on the partition of wind data, it says nothing about the degree of discrimination of the Senegal's daily rainfall on these clusters. There are various ways to estimate the discrimination of rainfall by cluster. The information criterion (IC) suggested by Santos *et al.* (2005) (Fig. 3b) is used for that purpose.

(1) $$IC = \sum_{i=1}^{k} \left| n_{i,r} - (p_r \times n_i) \right| .$$

Here $n_{i,r}$ is the number of days in cluster i that receive a rainfall amount greater than r, p_r is the probability of such rainy days in the whole population, n_i is the number of days in cluster i and k is the total number of clusters. Figure 3b shows I as a function of k for each station, together with the country average, using a threshold $r = 1$ mm. The information criterion I exhibits a large jump from 2 to 3 clusters, and a second smaller increase from 6 to 8 clusters. The curve is then almost flat from 8 to 10 clusters. We choose 8 clusters as a compromise between adequate discrimination of local rainfall, CI and the physical interpretation of the atmospheric circulation patterns.

b. Temporal sequence of weather types

The occurrence frequency of each WT varies on inter-annual time scales but also within each season. The mean seasonal cycle of each WT, the probabilities of transitions between them, and the spell-length distributions are illustrated in Fig. 4. The transition probabilities are tested using a Monte-Carlo test for transition matrix based on Markov chains (Vautard *et al.*, 1990). We generate 38 random time sequences of numbers from 1 to 8. Each sequence has a length of 92 time units and the total frequency of occurrence of each cluster is made to match the observed one. We then compute the transition matrix from this 38 time units x 92 days matrix and the process is repeated 10000 times. Observed transition probabilities exceeding the 99th percentile of their noise counterparts are taken to be statistically significant at the one-sided 99% level.

The occurrence of WT1, and especially that of WT7 & WT8, are strongly modulated by the seasonal cycle: WT1 is prevalent before about July 15, and WT7-8 after about September 15. WT1 also occurs during the core of the JAS season in persistent spells (e.g. 1968, 1972, 1977, 1978, 1981, 1986, and 1987, not shown). The WTs 2-6 are most prevalent from about July 10 to about September 20 but rarely persist for more than 5 days, except perhaps for WT2 (e.g. July 1975, July 1981, and August 1994, not shown). The transitions amongst the 5 WTs reveal preferred circuits: 2 → 3 → 4 → 2, and 3 → 4 → 6 → 5 → 3, and 2 → 5 → 3 → 4 → 2 (Fig. 4b), suggesting that these WTs may be associated with westward moving wave disturbances as AEWs. Inspection of the daily WT sequences for each year (not shown) indicates that these circuits typically last 3-9 days.

c. Atmospheric patterns

Composite maps of daily wind anomalies for the 8 weather types at 925, 700 hPa are presented in Figs. 5-8. The wind anomalies at 200 hPa are not shown since they mostly reflect the seasonal cycle of each cluster. These figures are organized following the mean seasonal evolution, with the early-season WT1 shown in Fig. 5, the WTs of the core JAS season displayed together in Figs 6-7 and the late-season WTs 7

and 8 shown in Fig. 8. The composites are plotted as standardized anomalies relative to the long-term July-September mean. Anomalies of divergence exceeding 0.25 standard deviations are shaded in Figs. 5-8, with standardized anomalies greater than 0.25 (light) and less than –0.25 (dark).Note that the maps cover a larger area than the window used in the clustering. A Student's T-test was applied to the wind anomalies in Figs. 5-8, with the number of effective degrees of freedom taken as the total number of days included in each composite divided by 10, to account for persistence. All of the main circulation features tested significant at the 99% confidence level using a two-sided test (not shown).

With respect to the July-September mean, WT1 is characterized by an anomalous anticyclone at 700hPa, centered to the west of Senegal (Fig. 5a), with strong surface northerly anomalies to the north, and an anomalous cyclonic center located near 5°W-20°N at 925 hPa (Fig. 5b). A region of anomalous convergence is located at 925 hPa over northern Senegal, with anomalous divergence above it at 700 hPa. A larger window indicates that this weather type is not particularly related to particular extratropical features (not shown). These features largely reflect mean conditions during early July when WT1 is prevalent, prior to the core monsoon season. However, similar composites result if the season is split into two, to consider the early (pre-July 16) and core parts of the season separately (not shown). Thus, WT1 may be associated with "breaks" during the core monsoon season, with circulation features typical of early July.

Weather types 2-6 all exhibit wavy patterns at 925 hPa (Fig. 6) and 700 hPa (Fig. 7) whose spatial structures are broadly consistent with westward-moving easterly wave disturbances (Burpee, 1972), when ordered according to the temporal sequences identified in Fig. 4b (Dhiedou *et al.*, 1998, 1999; Grist, 2002). WT3 is almost a mirror image of WT6 over the region used to define the clusters. In terms of horizontal structure at 700 hPa, the zonal wave length, horizontal phase tilts and meridional extent all exhibit the hallmarks of AEWs identified at 15°N in a previous study of ERA15 data by Kiladis *et al.* (2006); this is compatible with the location of the WT troughs and ridges in Fig. 7, whose centers at 700

hPa are located close to the latitude of the AEJ along 15°N. The anomalous convergence at 700hPa tends to be in phase with anomalous southerly winds, to the east of the trough axis. This is also consistent with AEWs identified at 15°N by Kiladis *et al.* (2006), while they found a different configuration at 10°N . Although they exhibiti these AEW characteristics, the patterns of WT2 and WT4 are also consistent with slower intra-seasonal modes, such as monsoon surges (Janicot and Sultan, 2001; Sultan *et al.*, 2003) over the western and central Sahel respectively. This is especially true for WT2, which is associated with long persistent spells (Fig. 4c), and exhibits a broader spatial scale, characterized by a strong meridional shear about the main axis of the AEJ, known to favor the development of squall lines (Fink and Reiner, 2003). At 200 hPa (not shown), WTs 2-4 are characterized by the broad-scale seasonal strengthening of the TEJ during JAS. At 200hPa, WTs 5-6 are characterized by weak anomalies over the western Sahel, with some evidence of wave patterns near 30°N (not shown).

In terms of low-level vertical structure, the troughs and ridges in WTs 2-6 exhibit an eastward tilt with height between 925 hPa and 700 hPa, and thus tilt against the mean vertical shear of the AEJ, consistent with positive baroclinic energy conversions, as seen in the AEW normal-mode calculations of Hall *et al.* (2006). In addition, the convergence anomalies at 700hPa tend to overly divergence anomalies at 925 hPa and vice versa, as found by Kiladis *et al.* (2006) in AEWs at 15°N. The WT composites of anomalous divergence change sign again at 200hPa (not shown). Differential vorticity advection by the mean vertical shear flow can account for this kind of vertical "checkerboard" structure in AEWs (Thorncroft and Hoskins, 1994), while rain evaporation may also contribute to the implied subsidence anomalies at 925hPa (Kiladis *et al.*, 2006).

Composites for the late-season WTs are shown in Fig. 8 over a broader region to highlight possible connections with the midlatitude circulation in the transition season. A strengthening and/or southward shift of the AEJ at 700hPa is visible near 9°N in both WTs (Fig. 8a,b). At 925 hPa, an anomalous anticyclonic center characterizes both WTs 7 and 8, with anomalous northeasterlies over western and

central Sahel (Fig. 8c,d). At 200 hPa, both WTs are characterized by a broad-scale westerly anomaly associated with the disappearance of the TEJ at the end of the JAS season (not shown, cf. Fig. 2e). A trough in the subtropical westerly jet near the African coast occurs in WT8, while a slight anomalous ridging there is found in WT7. These westerly anomalies are vertically extensive and visible at 700 hPa, though with large differences between states 7 and 8 over Senegal (Fig. 8a,b).This pattern could be associated with rainy events in boreal autumn, or even winter, from Senegal to Morocco (Knippertz, 2003; Knippertz and Martin, 2005). As for other weather types, there is again a vertical phase reversal in the anomalous divergence field between 700 and 925 hPa (Fig. 8).

d. Relationship between the weather states and rainfall occurrence

A central objective of this study is to relate the above circulation regimes to rainfall over Senegal. Figure 9 shows the spatial distribution of daily rainfall occurrence as anomalies relative to the long-term mean. Note that daily mean intensity of rainfall (i.e. mean rainfall amount during wet days > 1 mm) is poorly partitioned amongst the clusters (not shown). Weather types 1, 4 and 7 are the driest, and WTs 2, 5 and 6 the wettest. This basic differentiation is partly related to their seasonality since the seasonal cycle of rainfall (Fig. 1b,c) has been retained in the rainfall time series. However, WT1 is clearly identified with dry spells during the core of the JAS season as well (Fig. 4a). The westward moving wave WT sequences depicted in Figs. 6-7 are indeed consistent with a westward moving rain event. Station rainfall anomalies are broadly consistent with the accompanying divergence anomalies at 700 hPa (Figs. 5, 7-8). The positive rainfall anomalies in WT2, 5 and 6 coincide with anomalous convergence and southwesterly flow at 700 hPa, while the negative rainfall anomalies in WTs 1, 3 and 4 coincide with anomalous 700 hPa divergence and are located within the northerly or northwesterly anomalies at 700 hPa. These relationships are consistent with the findings of Kiladis *et al.* (2006) for AEWs identified at 15°N. WTs 7 and 8 are anomalously dry with respect to the seasonal average, consistent with their seasonality (Fig. 4a). However, WT8 is anomalously wet with respect to the late-September average.

e. Interannual variability of weather types and seasonal rainfall in Senegal

The connection between weather type and rainfall occurrence over Senegal suggests that it may be possible to use the weather types as a tool to interpret seasonal-scale rainfall anomalies in terms of year-to-year anomalies in weather-type frequency. In the following, "seasonal rainfall" will refer to seasonal rainfall occurrence frequency. Considering seasonal rainfall amounts instead of rainfall occurrence leads to similar results (not shown), but with slightly weaker relationships for amounts. This is consistent with the slightly higher spatial coherence and potential predictability of rainfall frequency compared to seasonal amount (Moron *et al.*, 2006, 2007a).

Figure 10 shows the relationship between the frequency occurrence of each WT and seasonal rainfall, for the 10 driest and wettest years, identified from the standardized anomaly index –*SAI*– of rainfall occurrence. The *SAI* is defined as the station-average of the standardized anomalies obtained by subtracting the mean and dividing by the interannual standard deviation at each station. For the "seasonal" WTs 1, 2 and 8, the differences in WT frequency between the two sets of years are consistent with the mean rainfall anomaly of each WT (Fig. 9). Thus the 10 driest years contain more of WT1 and 8, but less of WT2 (Fig. 10a-b,h).

Differences in frequency of WTs 4-7 are not significant overall between the wet and dry years, although shifts in WT seasonality can be identified (Fig. 10d-g). There are slightly more WT6 in dry years (Fig. 10f). Weather type 6 is associated with wet anomalies but its increased prevalence is concentrated in September, when rainfall occurrence is climatologically low (Fig. 1b). The relationship between WT3 and seasonal rainfall is complex. On average, this WT is accompanied by weakly negative rainfall anomalies (Fig. 9c), yet there are clearly more WT3 days in wet years than in dry years (Fig. 10c). This can be explained by differences in transition probabilities into WT3 (Fig. 4b) between the two sets of years, with more-frequent transitions from state 5 in dry years. WT3 days exhibit 10-40% higher rainfall probabilities when they follow WT2 as opposed to WT5.

f. Canonical correlation analysis

Year-to-year changes in WT frequency clearly cannot account for all interannual variability of rainfall. Even if the frequency of a WT remains constant, it may be associated with wetter conditions in some years than others. In this sub-section we estimate the relative importance of changes in WT frequency vs. changes in WT "character" (i.e. its rainfall characteristics), for interannual rainfall variability over Senegal. As in the preceding section, we confine our attention to rainfall occurrence only. Similar results are obtained using amounts, with a slight decrease of skill.

The number of wet days $N_{i,j}$ in year *i* at station *j* can be decomposed into the rainfall probability for each weather type $p_{i,j,k}$ in year *i* at station *j*, multiplied by the frequency of each weather type $n_{i,k}$ during that year

(2) $$N_{i,j} = \sum_{k=1}^{8} p_{i,j,k} n_{i,k} .$$

Two complementary Canonical Correlation Analyses (CCA, Barnett and Preisendorfer, 1987; Ward and Navarra, 1997; Moron *et al.*, 2001) are made to estimate the contribution of $n_{i,k}$ (i.e. WT frequency) and $p_{i,j,k}$ (i.e. WT character) in explaining $N_{i,j}$. The first CCA is made between $n_{i,k}$ and $N_{i,j}$, so that WT frequency is used to "predict" interannual variability in rainfall frequency. The second CCA uses $p_{i,j,k}$ averaged over stations as the predictor of $N_{i,j}$. Both CCAs are applied using cross-validation, leaving out 5 consecutive years each time, and computing the CCA on the remaining 33 years. We restrict our attention to the leading CCA mode in each case, since inclusion of subsequent modes is not found to significantly increase the skill.

Results of the first CCA between $n_{i,k}$ and $N_{i,j}$ are presented in Fig. 11, in terms of correlation between the "predicted" and observed rainfall occurrence frequency $N_{i,j}$ at each station (panel a), the loading of each WT's frequency $n_{i,k}$ (panel b), and the cross-validated CCA time scores (panel c). In panel (a), the "prediction" is equivalent to the cross-validated Model Output Statistic ("MOS") skill (Ward and Navarra, 1997; Moron *et al.*, 2001). The skill of WT frequency is spatially homogenous, with values between 0.36 and 0.60, except at Kedougou in the extreme SE of the country (Fig. 11a). The WT loadings are characterized by large positive loadings for WT2 and 3, and strong negative loadings for WT1 and WT8 (Fig. 11b). Thus, changes in WT frequency during the onset and end phases of the monsoon (WT1 and 8), breaks in the monsoon (WT1), and surges during the core of the JAS season (WT2) exert the largest impact on the interannual variability of rainfall frequency. This seasonality is brought out in the composite analysis of the 10 driest and wettest years in Fig. 10 which is consistent with the CCA result. Changes in the frequency of the WTs, interpreted mainly as phases of westward moving AEWs, on the other hand, are not significant in explaining the interannual variability of rainfall (Fig. 11b).

The temporal scores (Fig. 11c) suggest that the intensity of the link between WT frequency and rainfall occurrence has weakened since 1980. The correlation between both CCA time series is 0.60 for the whole period but drops from 0.81 in 1961-1979 to only 0.36 in 1980-1998.

Figure 12 presents the complementary CCA between $N_{i,j}$ and the year-to-year changes in the probability of rainfall within each weather type , averaged over stations $\overline{p_{i,j,k}}^{j}$. In this case rainfall probabilities enter into both $N_{i,j}$ and $\overline{p_{i,j,k}}^{j}$ so that the resulting "skill" should be interpreted as the extent to which interannual rainfall anomalies at the station level can be accounted for by year-to-year changes in average rainfall probability of each state, rather than evidence of predictability. The skill values, using $\overline{p_{i,j,k}}^{j}$ as the predictor (panel a) are somewhat higher than those in Fig. 11a, especially in the central-northern part

of Senegal. In this case, the loadings of each WT (panel b) are consistently positive with largest values for WTs whose frequency peaks in the core of the JAS season. The correlation between cross-validated CCA temporal scores is 0.80 (panel c) with similar values for the first and second halves of the time series (0.79 and 0.81 respectively).

The predictions of station-average *SAI* of rainfall occurrence made with the two CCA analyses are plotted in Fig. 13, together with the observed *SAI*. The two predictions are seen to be quite independent (r = 0.28). During certain years, such as the 1972 dry year, the contribution of WT frequency is particularly large, mostly associated with an abundance of "dry" WT1 (41 days) and no wet WT2. However, the discrepancy between observed SAI and its prediction from WT-frequency is large in 1965, 1980, 1982, 1987, 1991 and 1992, where year-to-year changes in $p_{i,j,k}$ are clearly important. The low-frequency component of the CCA predictions is plotted in Fig. 13b. Changes in WT-character $p_{i,j,k}$ seem more important in accounting for decadal variability of rainfall frequency over the Sahel.

g. Relationships with sea surface temperature

To gain further insight, we plot correlations between the CCA modes and SST in Fig. 14. Correlations with the observed *SAI* (panel a) show the well-known SSTA structure familiar from previous analyses of Sahelian rainfall (i.e. Fontaine and Bigot, 1993; Rowell *et al.*, 1995; Ward, 1998; Janicot *et al.*, 2001). Positive rainfall anomalies are associated with La Niña-like SST anomalies over the tropical Pacific, cold SSTAs over the Indian Ocean and warm SSTAs over the tropical North Atlantic. As noted by Rowell (2001), the highest correlations in tropical Pacific are shifted south of the equator relative to the canonical ENSO SST pattern (Rasmusson and Carpenter, 1982). The fact that correlations are weak over the Atlantic in Fig. 14a could be associated with the relatively short period of the analysis and also the stronger link between Tropical Atlantic and Sahelian rainfall in 1950-70 than thereafter (Ward, 1998;

Janicot *et al.*, 2001). This would tend to underemphasize the multi-decadal variability, which is strongly correlated with Atlantic SSTAs (Folland *et al.*, 1986; Rowell *et al.*, 1995).

The SST correlations with the leading CCA mode of WT frequency (Fig. 14b) are very clearly dominated by ENSO. The correlations over the Tropical Pacific are now almost symmetric relative to the equator and match the canonical ENSO pattern (Rasmusson and Carpenter, 1982). This pattern also matches the correlations between high-frequency (< 8 years) variations of regional Sahelian index and SST (Rowell *et al.*, 1995; Ward, 1998). In contrast, the SST correlations with the complementary leading CCA mode of WT character (Fig. 14c) tend to resemble the other aspects of the correlations with the SAI over the Atlantic, west Pacific and Indian Oceans. Indeed, the correlation pattern in Fig. 14c resembles the low-frequency (> 8 years) SST pattern identified by Rowell *et al.* (1995) and Ward (1998). Over the tropical Pacific, the equatorial correlations are close to zero, with the highest values clearly shifted south of the equator.

The analysis of SST correlations provides further evidence that the influence of ENSO on Senegal rainfall is largely through changes in WT frequency, while the character of the rainfall associated with the WTs themselves undergoes important modulation at decadal time scales.

4. Summary and discussion

a. Summary

An objective classification procedure using the *k*-means algorithm was used to summarize the unfiltered daily atmospheric variability during the boreal summer season 1961-1998 over the western Sahel and eastern Tropical North Atlantic (0°-30°W, 5°-25°N). The clustering scheme was based on regional gridded wind fields from the daily ERA-40 reanalyses of the monsoon flow at 925 hPa, the African Easterly Jet level at 700 hPa and the Tropical Easterly Jet level at 200 hPa. An 8-cluster solution was

shown to offer a good balance between the discrimination of daily rainfall (Fig. 9) and physical interpretation of the associated atmospheric circulation patterns (Figs. 5-8).

Three of the weather types were found to correspond primarily to the onset (WT1, Fig. 5) and end of the monsoon season (WTs 7-8, Fig. 8). WT1 was also found to be associated with dry spells during the core of the JAS season (Fig. 4). WT8 may be associated with late-season interactions with the extratropics (Fig. 8), leading to scattered rainfall mainly over NW Senegal.

Weather types 2-6 were found to be primarily associated with westward moving easterly waves and monsoon surges (Fig. 6-7). They are most prevalent from mid-July to mid-September (Fig. 4a) and are generally less persistent than WT1, 7 and 8, with the exception of WT2 (Fig. 4c). Two main circuits of transition between these weather types were identified, with $2 \rightarrow 3 \rightarrow 4 \rightarrow 2$ predominant during the first part of the JAS season, and $3 \rightarrow 4 \rightarrow 6 \rightarrow 5 \rightarrow 3$ during the second part (Fig. 4b). Both circuits are consistent with a westward-moving easterly waves (period 3-9 days and wavelength 2000-3000 km). WT2 exhibits longer spells of 3-7 days (Fig. 4c) and a pattern characteristic of the monsoon surge over western Sahel (Fig. 6a).

Weather types 2, 5 and 6 were found to be characterized by anomalously high rainfall occurrence over Senegal (Fig. 9b,e,f) with WT3, and particularly WT4, being anomalously dry (Fig. 9c,d). However, these relationships with rainfall are not unique. For example, WT3 tends to be anomalously dry when it follows WT5, but anomalously wet when it follows WT2. The more frequent $5 \rightarrow 3$ transition leads to a weak negative mean rainfall anomaly associated with WT3 (Fig. 9c). Note that mean daily intensity is poorly partitioned amongst the clusters, consistent with the spatial coherence at interannual scale being primarily conveyed by the frequency of occurrence (Moron *et al.*, 2006, 2007a).

Canonical correlation analysis was used to quantify the extent to which the interannual variability of rainfall occurrence is related to the occurrence-frequency of weather types versus year-to-year changes in the rainfall character of the weather types. The frequency of early and late-season weather types (WT1, 7 and8), as well as the frequency of the long-lasting spells of WT2, were found to be strongly related to seasonal-average frequency of wet days > 1 mm, particularly in central and northern Senegal. By contrast, the frequencies of westward moving wave disturbances (WTs 4-6), were not found to have a significant impact on interannual rainfall variability (Figs. 11-12), consistent with previous findings (i.e. Rowell, 2001: Fink and Reiner, 2003; Fink *et al.* 2004).

The component of seasonal rainfall associated with changes in WT frequency was found to be strongly related to ENSO (Fig. 14b). El Niño events tend to be associated with more (less) WT1, 7 & 8 (WT2 & 3) and vice-versa for La Niña events. The complementary component not explained by weather-type frequency is characterized by a consistent increase/decrease of probability of rainfall for each WT, especially those that occur during the core of the JAS season (Fig. 14c). This signal explains a larger part of the interannual variance of the country-averaged rainfall occurrence. It was found to be less related to ENSO, and to have a stronger decadal component.

b. Discussion

Our findings demonstrate that weather typing using cluster analysis of daily circulation fields over the western Sahel and neighboring Tropical Northern Atlantic is able to recover the main features of circulation variability, without the need to resort to explicit time filtering of the data, as is commonly done. The resulting description gives an integrated view of the complex regional-scale atmospheric circulation features on a mix of different spatial (e.g. meridional migration of the ITCZ, westward moving easterly waves, persistent monsoon surges and breaks, tropical-extratropical interactions) and temporal (e.g. seasonal cycle, sub-seasonal variability etc.) scales. Weather type 1, is of particular interest in this respect, being associated with both the pre-monsoonal seasonal dryness in early July, as well as monsoon

breaks during the core monsoon season. Weather types 2-6 show many of the hallmarks of the AEW regression patterns constructed from filtered ERA15 data by Kiladis *et al.* (2006), when the base point was chosen to be at 15°N – consistent with the latitude of the wave centers of the weather types. Thus, positive rainfall anomalies (WTs 2,5 & 6) are associated with anomalous convergence and southwesterly flow at 700 hPa. Below this level, the sign of the divergence anomalies reverses. This phase reversal was found previously for the AEWs identified at 15°N by Kiladis *et al.* (2006), and interpreted in terms of waves on a vertical shear flow. All of our WTs exhibit this structure south of 25°N.

From the methodological point of view, using discrete clusters to represent propagating atmospheric patterns as AEWs could be questioned. For a certain level of discretization, identified here as 6-7 clusters (Fig. 3), distinct weather types mostly represent different phases of the same propagating meteorological feature. The flatness of the classifiability index between 6 and 10 clusters suggests that AEWs will be represented by additional weather types as the number of clusters grows. In this context, the weather types should be interpreted as composite "snapshots" of the different phases of the same atmospheric phenomenon, rather than as distinct atmospheric phenomenon. On the other hand, our approach, which provides a straightforward and objective partitioning of the unfiltered atmospheric variability at various timescales, may be advantageous over Senegal where there is a complex interaction between AEW and monsoonal processes. Thus, the classical AEW normal-mode structure with ascent in the northerlies (Thorncroft and Hoskins 1994; Hall *et al.* 2006) is not what would be expected in a monsoon surge. Observational AEW studies paint a more complex picture; for example Kiladis *et al.* (2006) found ascent in various phases of waves identified at 10°N, while waves identified at 15°N exhibited ascent consistently in the southerlies. Our results are consistent with the latter which may reflect the mix of AEW and monsoonal processes.

The discrimination of station rainfall frequency by the circulation-based weather types appears promising, but it will be of interest to compare the benefits of this approach with a state classification based directly

on the station rainfall observations themselves, such as with hidden Markov models –HMM– (e.g., Robertson *et al.*, 2006). A match between weather-typing and HMM state classifications would only be expected if local-scale rainfall is uniquely conditioned by the larger scale atmospheric circulation. On the other hand, two similar regional-scale patterns may not necessarily be associated with the same station rainfall pattern and vice-versa. The degree of complexity may vary significantly across the Tropics, depending on the rainfall-generating phenomena. The performance of weather typing and HMM approaches to downscaling from a GCM is explored in part II of this study.

A potentially important result provided by the weather typing is the separation of interannual rainfall variance into a component that is associated with year-to-year changes in weather-type frequency, and a component that is not. The component of rainfall associated with weather-type frequency largely accounts for the relationship with between Senegal rainfall and ENSO. The weather types more prevalent during warm ENSO events are all associated with enhanced north-easterlies at low levels over the western Sahel and/or the neighboring Tropical North Atlantic, consistent with previous findings at the seasonal time scale (i.e. Trzaska *et al.*, 1996; Janicot *et al.*, 1998, 2001; Rowell, 2001). Our finding that seasonal rainfall anomalies associated with year-to-year changes in the frequency of westward moving wave weather types is unrelated to ENSO is consistent with the conclusion of Rowell (2001). The relationship between the weather-type frequency and rainfall variability appears to weaken after 1980, and further work is needed to determine whether this is more than just random sampling variability (Moron *et al.*, 2003; Moron, 2005).

The component of country-averaged rainfall occurrence not associated with weather-type frequency accounts for a larger part of the interannual rainfall variance. It appears to be stronger on longer time scales, and may be the key factor in accounting for trends in Sahelian rainfall. This component could perhaps be associated with a large-scale variation of a circulation-independent process linked to rainfall, such as the availability of moisture, while the ENSO teleconnection is more dynamical. However, the

interpretation remains speculative because of the short 1961-98 record of daily station rainfall available. The relationship between the rainfall character of the weather types and other reanalysis variables remains to be explored.

This study provides a framework for downscaling the local rainfall from atmospheric circulation patterns. If a GCM is able to simulate these weather types sufficiently accurately, together with aspects of their temporal variability, transfer functions could be used to associate these regional-scale patterns with local-scale rainfall. This is explored in Part II of this paper.

Acknowledgments

We would like to thank DMN-Senegal for providing the daily rainfall dataset for Senegal and B. Fontaine, B. Sultan, P. Knippertz, A. Giannini and S. Trzaska for their insightful comments at various stages of this study. We thank also the editor (David Straus) and the four anonymous reviewers whose constructive comments lead to a substantially improved manuscript. ECMWF ERA-40 wind data used in this study have been obtained from the ECMWF data server (http://data.ecmwf.int/data/d/era40_daily/). This research was supported by NOAA through a block grant to the International Research Institute for Climate and Society (IRI), and by Department of Energy grant DE-FG02-02ER63413.

References

Barnett T.P., and R. Preisendorfer, 1987: Origins and levels of monthly and seasonal forecast skill for united-states surface air temperatures determined by canonical correlation analysis. *Mon. Wea Rev.*, **115**, 1825-1850.

Burpee R.W., 1972: The origin and structure of easterly waves in the lower troposphere in North Africa. *J. Atmos. Sci,* **29**, 77-90.

Camberlin P., and M. Diop, 1999: Interrelationships between groundnut yield in Senegal, Interannual rainfall variability and sea surface temperatures. *Theor. Appl. Climatol*., **63**, 163-181.

Camberlin P., and M. Diop, 2003: Application of daily rainfall principal component analysis to the assessment of the rainy season characteristics in Senegal. *Climate Research*, **23**, 159-168.

D'Amato N., and T. Lebel, 1998: On the characteristics of the rainfall events in the Sahel with a view to the analysis of the climatic variability. *Int. J. Climatol*., **18**, 955-974.

Diday E., and J.C. Simon, 1976: Clustering analysis. In Digital Pattern recognition, Fu KS (editor) Communication and cybernetics, Vol. 10, Springer-Verlag, 47-94.

Diedhiou A., S. Janicot, A. Viltard, and P. De Felice, 1998: Evidence of two states of easterly waves over West-Africa and Tropical Atlantic, *Geophys. Res. Letters*, **25**, 2805-2808.

Diedhiou A., S. Janicot, A. Viltard, P. De Felice, and H. Laurent, 1999: easterly wave states and associated convection over West-Africa and tropical Atlantic: results from the NCEP/NCAR and ECMWF reanalyses. *Clim. Dyn.*, **15**, 795-822.

Diedhiou A., S. Janicot, A. Viltard, and P. De Felice, 2001: Composite patterns of easterly disturbances over West-Africa and the tropical Atlantic: a climatology from the 1979-1995 NCEP/NCAR reanalyses. *Clim. Dyn.*, **18**, 241-253.

Druyan L.M., M. Fukaleza, and P. Lonergan, 2006: Mesoscale analyses of West-African summer climate: focus on wave disturbances. *Clim. Dyn.*, **24**, doi:10.1007/s00382-006-0141-9.

Ebisuzaki W., 1997: A method to estimate the statistical significance of a correlation when the data are serially correlated. *J. Climate*, **10**, 2147-2153.

Fink A.H., and A. Reiner, 2003: Spatio-temporal variability of the relation between African easterly waves and West African Squall lines in 1998 and 1999. *J. Geophys. Res.*, **108**, D114332, doi:10.1029/2002JD002816.

Fink A.H., D.G. Vincent, P. Reiner, and P. Speth, 2004: Mean state and wave disturbances during phase I, II and III of GATE based on ERA-40. *Mon. Wea. Rev.*, **132**, 1661-1683.

Folland C.K., T.N. Palmer, and D.E. Parker, 1986: Sahel rainfall and worldwide sea temperatures. *Nature*, **320**, 602-607.

Fontaine B., and S. Bigot, 1993: West-African rainfall deficits and sea surface temperatures, *Int. J. Climatol.*, **13**, 271-285.

Ghil M., and A.W. Robertson, 2002: "Waves" vs. "particles" in the atmosphere's phase space: A pathway to long-range forecasting. *Proc. Nat. Acad. Sci*, **99**, 2493-2500.

Giannini A., R. Saranavan, and P. Chang, 2003: Oceanic forcing of Sahel rainfall on interannual to interdecadal timescales, *Science*, **302**, 1027-1030.

Grist J.P., 2002: Easterly waves over Africa. Part I: the seasonal cycle and contrasts between wet and dry years. *Mon. Wea. Rev.*, **130**, 197-211.

Gu G., and R.F. Adler, 2004: Seasonal evolution and variability associated with the West-African monsoon system. *J. Climate*, **17**, 3364-3377.

Gu G., R.F Adler, G.J Huffman, and S. Curtis, 2004: African easterly waves and their association with precipitation. *J. Geophys. Res.*, **109**, D04101, doi:10.1029/2003JD003967.

Hall, N. M. J., G. K. Kiladis, and C. D. Thorncroft, 2006: Three-dimensional structure and dynamics of African easterly waves. Part II: Dynamical modes. *J. Atmos. Sci.*, **63**, 2231-2245.

Hastenrath S., 1984: Interannual variability and annual cycle: mechanisms of circulation and climate in the tropical Atlantic. *Mon. Wea. Rev.*, **112**, 1097-1107.

Hastenrath S., 1990: Decadal scale changes of the circulation in the tropical Atlantic sector associated with Sahel drought. *Int. J. Climatol.*, **10**, 459-472.

Janicot S., V.Moron, and B. Fontaine, 1996: Sahel drought and ENSO dynamics. *Geophys. Res. Letters*, **23**, 515-518.

Janicot S., A. Harzallah, B. Fontaine, and V. Moron, 1998: West African monsoon dynamics and eastern equatorial Atlantic and Pacific SST anomalies (1970-1988). *J. Climate*, **11**, 1874-1882.

Janicot S., and B. Sultan, 2001: Intra-seasonal modulation of convection in the West-African monsoon. *Geophys. Res. Letters*, **28**, 523-526.

Janicot S., P. Camberlin and I. Poccard, 2001: Summer Sahel-ENSO teleconnection and decadal time scale SST variations. *Climate Dyn.*, **16**, 272-289.

Kiladis G.N., C.D. Thorncroft, and N.M.J. Hall, 2006: Three dimensional structure and dynamics of African Easterly waves. Part I: observations. *J. Atmos. Sci.*, **63**, 2212-2230.

Knippertz P., 2003: Tropical-extratropical interactions causing precipitation in northwest Africa: Statistical analysis and seasonal variations, *Mon. Wea. Rev.*, **131**, 3069-3076.

Knippertz P., and J.E. Martin, 2005: Tropical plumes and extreme precipitation in subtropical and tropical West Africa, *Quart. J. Meteo. Soc.*, **131**, 2337-2361.

Lamb P.J., 1978: Large-scale tropical Atlantic surface circulation patterns associated with Subsaharan weather anomalies, *Tellus A*, **30**, 240-251.

Laurent H., N. D'Amato, and T. Lebel, 1998: How important is the contribution of the mesoscale convective complexes in the Sahelian rainfall ? *Phys. Chem. Earth*, **23**, 629-633.

Lavaysse C., A. Diedhiou, H. Laurent, and T. Lebel, 2006: African easterly waves and convective activity in wet and dry sequences of the West African monsoon. *Clim. Dyn.*, **27**, 319-332.

Lebel T., A. Diedhiou, and H. Laurent, 2003: Seasonal cycle and interannual variability of the sahelian rainfall at hydrological scales. *J. Geophys. Res.*, **108**, doi:10.1029/2001JD001580.

Louvet S., B. Fontaine and P. Roucou, 2003: Active phases and pauses during the installation of the West-African monsoon through 5-day CMAP rainfall (1979-2001). *Geophys. Res. Letters*, **30**, 2271, doi:10.1029/2003GL018058

Matthews A.J., 2004: Intraseasonal variability over Tropical Africa during northern summer. *J. Climate*, **17**, 2427-2440.

Michelangeli P.A., R. Vautard, and B. Legras, 1995: Weather regimes – recurrence and quasi-stationnarity, *J. Atmos. Sci.*, **52**, 1237-1256.

Mo K.T., and M. Ghil, 1988: Cluster analysis of multiple planetary flow regimes, *J. Geophys. Res.*, **93**, 10927-10952.

Molteni F., S. Tibaldi, and T.N. Palmer, 1990: Regimes in the wintertime circulation over Northern extratropics. 1. Observational evidence. *Quart. J. Meteo. Soc.*, **116**, 31-67.

Moron V., 1994: Guinean and sahelian rainfall anomaly indices at annual and monthly time scales (1933-1990), *Int. J. Climatol*., **14**, 325-341.

Moron V., A. Navarra, M.N. Ward, and E. Roeckner, 1998: Skill and reproductibility of seasonal rainfall patterns in the tropics in ECHAM-4 GCM simulations with prescribed SST, *Clim. Dyn.*, **14**, 83-100.

Moron V., A. Navarra, and M.N. Ward, 2001: Observed and SST-forced seasonal rainfall variability across Tropical America. *Int. J. Climatol.*, **21**, 1467-1501.

Moron V., Philippon N., and B. Fontaine, 2003: Skill of Sahel rainfall variability in four atmospheric GCMs forced by prescribed SST, *Geophys. Res. Letters*, **30**, 2221, doi:10.1029/2003GL018006.

Moron V., Philippon N., and B. Fontaine, 2004: Simulation of West-African monsoon circulation in four atmospheric general circulation models forced by prescribed sea surface temperatures, *J. Geophys. Res.*, **109**, D24105, doi:10.1029/2004JD004760.

Moron V., 2005: Skill of sahelian rainfall index in two atmospheric general circulation models ensemble forced by prescribed sea surface temperatures. *CLIVAR exchanges*, **33**, 14-19.

Moron V., A.W. Robertson, and M.N Ward, 2006: Seasonal predictability and spatial coherence of rainfall characteristics in the tropical setting of Senegal. *Mon. Wea. Rev.*, **134**, 3248-3262..

Moron V., A.W. Robertson, M.N. Ward, and P. Camberlin, 2007a : Spatial coherence of tropical rainfall at regional scales. *J. Climate*, in press.

Moron V., A.W. Robertson, M.N. Ward, and O. Ndiaye, 2007b : Weather types and rainfall in Senegal. Part II: Downscaling with local scaling, k nearest neighbor analog, weather classification and hidden Markov models. *J. Climate,* sub judice.

Nicholson S.E., 1979: Revised rainfall series for the West-African subtropics, *Mon. Wea. Rev.*, **107**, 620-623.

Paeth H., and P. Friederichs, 2004: Seasonality and time scales in the relationship between global SST and African rainfall, *Clim. Dyn.*, **23**, 815-837.

Plaut G., Simonnet E., 2001: Large-scale circulation classification, weather regimes and local climate over France, the Alps and western Europe, *Clim. Res.*, **17**, 303-324.

Rasmusson E.M., and T.H. Carpenter, 1982: Variations in tropical sea-surface temperature and surface wind fields associated with the southern oscillation El-Nino. *Mon. Wea. Rev.*, **110**, 354-384.

Robertson A.W., and M. Ghil, 1999: Large-Scale Weather Regimes and Local Climate Over the Western United States. *J. Climate*, **12**, 1796-1813

Robertson, A. W., and C. R. Mechoso, 2003: Circulation Regimes and Low-Frequency Oscillations in the South Pacific Sector. *Mon. Wea. Rev.,* **131**, 1566-1576.

Robertson A. W., S. Kirshner, P. Smyth, S.P. Charles, and B.C. Bates, 2006: Subseasonal-to-Interdecadal Variability of the Australian Monsoon Over North Queensland. *Quart. J. Royal Meteor. Soc.,* **132***,* 519-542.

Rowell D.P., C.K. Folland, K. Maskell, and M.N. Ward, 1995: Variability of summer rainfall over tropical North Africa (1906-1992) : observations and modelling. *Quart. J. Meteo. Soc.*, **113**, 669-704.

Rowell D.P., 2001: Teleconnections between the tropical Pacific and the Sahel. *Quart. J. Meteo. Soc.*, **127**, 1683-1706.

Santos J.A., J. Corte-Real, and S.M. Leite, 2005: Weather regimes and their connection to the winter rainfall in Portugal, *Int. J. Climatol.*, **25**, 33-50.

Simmons A.J., and J.K. Gibson, 2000: The ERA-40 project plan, ERA-40 project report series n 1, ECMWF, Reading, 63 pp.

Sperber K.R. and T.N. Palmer, 1996: Inter-annual tropical rainfall variability in General Circulation Model simulations associated with the Atmospheric Model Intercomparison Project. *J. Climate*, **9**, 2727-2750.

Sultan B., and S. Janicot, 2000: Abrupt shift of the ITCZ over West-Africa and intra-seasonal variability. *Geophys. Res. Letters*, **27**, 3353-3356.

Sultan B., S. Janicot, and A. Diedhiou, 2003: The West-African monsoon dynamics. Part I : documentation of intra-seasonal variability. *J. Climate*, **16**, 3389-3405.

Taleb E.H., Druyan L.M., 2003: Relationships between rainfall and West African wave disturbances in station observations. *Int. J. of Climatol.*, **23**, 305-313.

Thorncroft C.D., and B. J. Hoskins, 1994: An idealized study of African easterly waves I: A linear view. *Quart. J. Roy. Meteor. Soc.*, **120**, 953-982.

Thorncroft C.D., and D.P. Rowell, 1998: Interannual variability of African wave activity in a general circulation model. *Int. J. Climatol.*, **18**, 1305-1323.

Trzaska S., V. Moron, and B. Fontaine, 1996: Global atmospheric response to specific linear combination of the main SST modes. Part I: numerical experiments and preliminary results. *Ann. Geophysicae*, **14**, 1066-1077.

Vautard R, Mo K.C., and M. Ghil, 1990: Statistical significance test for transition matrices of atmospheric Markov chains. *J. Atmos. Sci.*, **47**, 1926-1931.

Ward M.N., and A. Navarra, 1997: Pattern analysis of SST-forced variability in ensemble GCM simulations: Examples over Europe and the tropical Pacific. *J. Climate*, **10**, 2210-2220.

Ward M.N., 1998: Diagnosis and short-lead time prediction of summer rainfall in tropical North Africa at interannual and multidecadal timescales. *J. Climate*, **11**, 3167-3191.

Figure captions

Figure 1: (a) Map location of the 13 stations, (b) mean daily rainfall frequency (in % of wet days receiving more than 1 mm of rainfall) at each station and (c) mean daily rainfall amounts (in mm / day in wet days) for the 13 stations of the observed network. The curves represent a smoothed seasonal cycle (low-pass recursive filter retaining only frequencies lower than 1/30 cycle-per-day). The number refers to each station on the location map (a) (1: Podor, 2: St Louis, 3: Linguere, 4: Dakar-Yoff, 5: Diourbel, 6: Kaolack, 7: Goudiry, 8: Kounghel, 9: Tambacounda, 10: Kolda, 11: Kedougou, 12: Diouloulou, 13: Ziguinchor).

Figure 2: Climatological mean of ERA-40 winds in July-September 1961-1998 (a) 200 hPa; (b) 700 hPa and (c) 925 hPa. The right column displays the seasonal cycle (= mean of daily values filtered by a low-pass recursive filter retaining only frequencies lower than 1/30 cycle-per-day) of the (d) 200 hPa, (e) 700 hPa and (f) 925 hPa winds averaged over the 9 grid-points covering Senegal (i.e. 12.5°-17.5°W and 12.5°-17.5°N) delineated as a black box on panels (a-c).

Figure 3: (a) Classifiability Index – CI – (Michelangeli *et al.*, 1995) for 2-10 clusters (bold line with circle) defined with *k*-means on the 7 leading principal components (PCs) of zonal and meridional components of ERA-40 winds at 925, 700 and 200 hPa. The dashed line give the CI two-sided 90% confidence interval extracted from 100 simulations with red noise having the same covariance at lag 0 and 1 as the 7 leading PCs of wind data. (b) Information Criterion (Santos *et al.*, 2005) computed on daily rainfall with a threshold of 1 mm. Each station is displayed as a thin line while the bold line with dots represents the country average. The 2-10 clusters are defined with k-means on the 7 leading principal components of zonal and meridional components of ERA-40 winds at 925, 700 and 200 hPa.

Figure 4: (a) Seasonal variation of the weather types (WT). The seasonal cycle (= mean of daily value) is smoothed by a low-pass filter retaining periods lower than 1/30 cycle-per-day; (b) probability transition between the weather types The arrows indicate the transition that occurs more likely than chance at the one-sided 99% level (Vautard *et al.*, 1990) and the circles around the weather types is proportional to the

one-day persistence (i.e. the probability that a WT on day *d* is the same on day *d*+1); (c) % of days of each types included in homogenous spells lasting at least 3, 5 and 7 days.

Figure 5: Composite maps of (a) 700 hPa, and (b) 925 hPa anomaly winds of weather type (WT) 1. The raw data from July, 1961 to September 30, 1998 are normalized to zero mean and unit variance before the computation of the composite. Shading indicates composite anomalies of divergence greater than 0.25 (light) and less than –0.25 (dark). Divergence (*D*) is computed from the raw zonal (*u*) and meridional (*v*) winds in Cartesian coordinates ($D = \frac{du}{dx} + \frac{dv}{dy}$) and then standardized to zero mean and unit variance. Positive (negative) values indicate anomalous divergence (convergence). The weather types are computed from wind data in 30°W-0°; 2.5°-27.5°N delineated by a dashed black box.

Figure 6: Composite maps of 925 hPa anomaly winds for (a) weather type (WT) 2, (b) WT3, (c) WT4 (d), WT5 and (e) WT6. Shading indicates composite anomalies of divergence greater than 0.25 (light) and less than –0.25 (dark). Details as in Fig. 5.

Figure 7: Same as Fig. 6 for 700 hPa anomaly winds.

Figure 8: Composite maps of anomaly winds and divergence for weather types (WT) 7 and 8: (a) 700 hPa for WT7, (b) 700 hPa for WT8, (c) 925 hPa for WT7, (d) 925 hPa for WT8. Details as in Fig. 5.

Figure 9: Rainfall occurrence anomalies (in %) associated for (a) weather type (WT) 1, (b) WT2, (c) WT3, (d) WT4, (e) WT5, (f) WT6, (g) WT7, (h) WT8. Significant values at the one-sided 99% level according to a chi-square test (null hypothesis is that the probability of rainfall > 1 mm during the days belonging to a given WT is the same as the one of the remaining days) are filled in black.

Figure 10: Mean seasonal cycle of weather type (WT) frequency for the 10 driest (full line) and 10 wettest (dashed line) July-September seasons. The selected seasons are determined from the standardized anomaly index of rainfall occurrence (see text). The WT frequency was computed on a daily basis from each sample of 10 years, and then smoothed for clarity using a recursive low-pass filter retaining only frequencies lower than 1/30 cycle-per-day. A dot on each curve indicates a significant difference between both samples at the two-sided 95% level according to a Student's T test (the null hypothesis is that the

mean frequency of both samples is equal). The mean occurrence frequency for each WT during the 10 driest and 10 wettest seasons are indicated (in days per July-September season) in the upper right corner of each panel, along with the Student's T Test p-value of the difference between dry and wet samples

Figure 11: Leading mode of a cross-validated CCA between interannual anomalies of weather type frequency and station rainfall frequency ; (a) correlations x 100 between the observed and "predicted" rainfall frequency ; (b) homogeneous correlation of weather type frequency ; (c) CCA time series of weather type frequency (dashed line and square) and station rainfall frequency (solid line and circle) in standardized values. The homogenous correlations in (b) are the correlations between weather type frequency and the cross-validated time series associated with its CCA pattern (dashed line in panel c).

Figure 12: Leading mode of a cross-validated CCA between interannual anomalies of the average rainfall probability within each weather type and station rainfall frequency; (a) correlations between the observed and "predicted" rainfall frequency ; (b) homogeneous correlation of weather type average rainfall probability; (c) CCA time series of weather type average rainfall probability (dashed line and square) and frequency of occurrence of rainfall (solid line and circle) in standardized values. The homogenous correlations in (b) are the correlations between rainfall probability within each weather type and the cross-validated time series associated with its CCA pattern (dashed line in panel c).

Figure 13: (a) Standardized anomaly index (*SAI*) of observed rainfall frequency (thick line), estimated rainfall frequency hindcast by the CCA between rainfall frequency and average probability of rainfall occurrence of each weather type (full line + circle), and by the CCA between rainfall frequency and weather type frequency (dotted line + square). (b) Same as (a) for the low-frequency component. The low-frequency is extracted by a recursive low-pass filter removing high frequencies higher than 1/8 cycle-per-year.

Figure 14: Correlation between observed SST in July-September and (a) observed standardized anomaly index (*SAI*) (from rainfall occurrence > 1 mm), (b) leading CCA mode of the weather type frequency (dashed line with squares in Fig. 11c) and (c) leading CCA mode of the average probability of rainfall of each weather type (dashed line with squares in Fig. 12c). The contours are indicated at -0.6, -0.4, -0.2, 0,

0.2, 0.4, 0.6 and shadings indicate local significant correlations at the two-sided 95% level according to a random-phase test (Janicot *et al.*, 1996; Ebisuzaki, 1997).

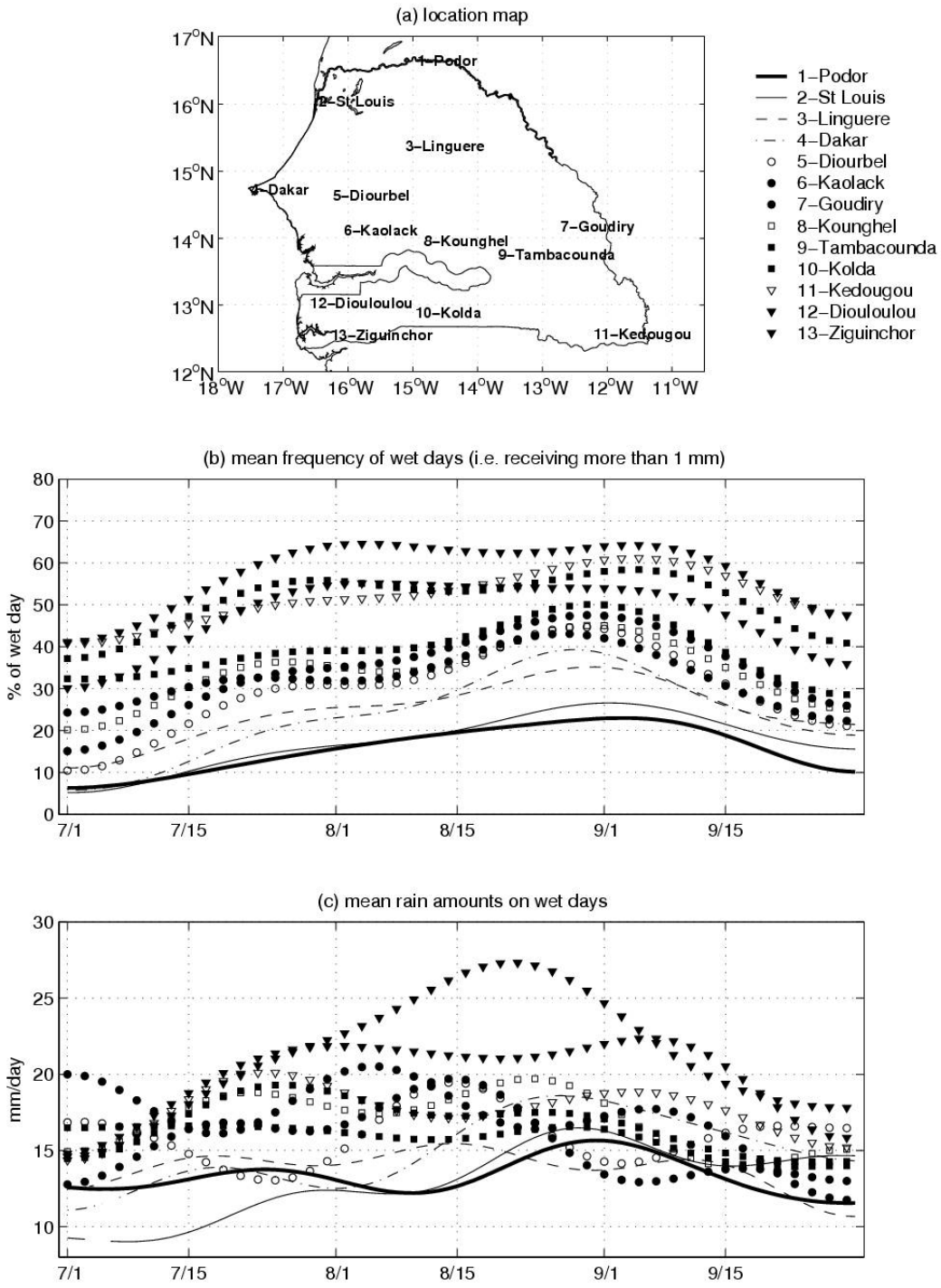

Figure 1: (a) Map location of the 13 stations, (b) mean daily rainfall frequency (in % of wet days receiving more than 1 mm of rainfall) at each station and (c) mean daily rainfall amounts (in mm / day in wet days) for the 13 stations of the observed network. The curves represent a smoothed seasonal cycle (low-pass recursive filter retaining only frequencies lower than 1/30 cycle-per-day). The number refers to each station on the location map (a) (1: Podor, 2: St Louis, 3: Linguere, 4: Dakar-Yoff, 5: Diourbel, 6: Kaolack, 7: Goudiry, 8: Kounghel, 9: Tambacounda, 10: Kolda, 11: Kedougou, 12: Diouloulou, 13: Ziguinchor).

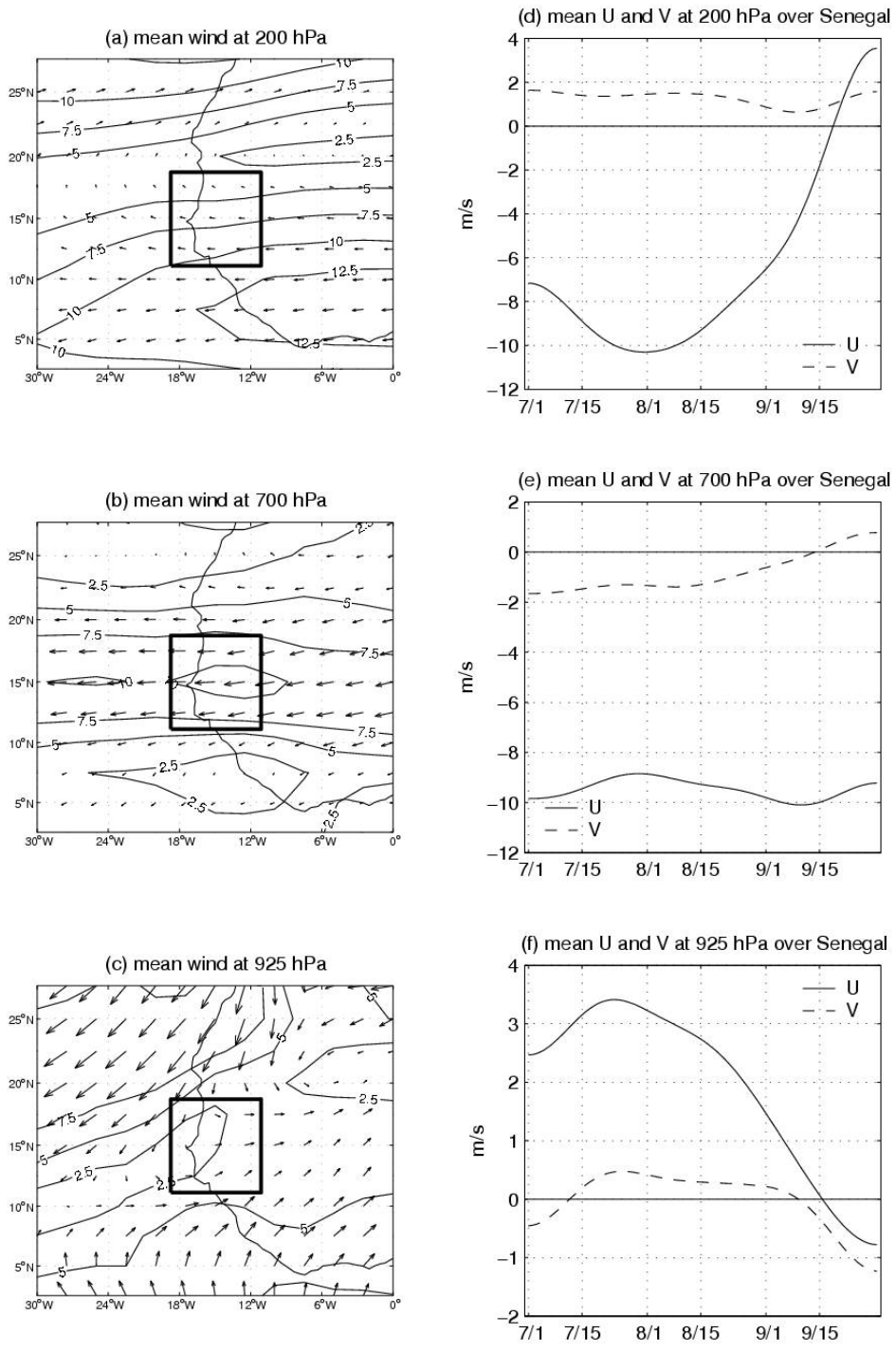

Figure 2: Climatological mean of ERA-40 winds in July-September 1961-1998 (a) 200 hPa; (b) 700 hPa and (c) 925 hPa. The right column displays the seasonal cycle (= mean of daily values filtered by a low-pass recursive filter retaining only frequencies lower than 1/30 cycle-per-day) of the (d) 200 hPa, (e) 700 hPa and (f) 925 hPa winds averaged over the 9 grid-points covering Senegal (i.e. 12.5°-17.5°W and 12.5°-17.5°N) delineated as a black box on panels (a-c).

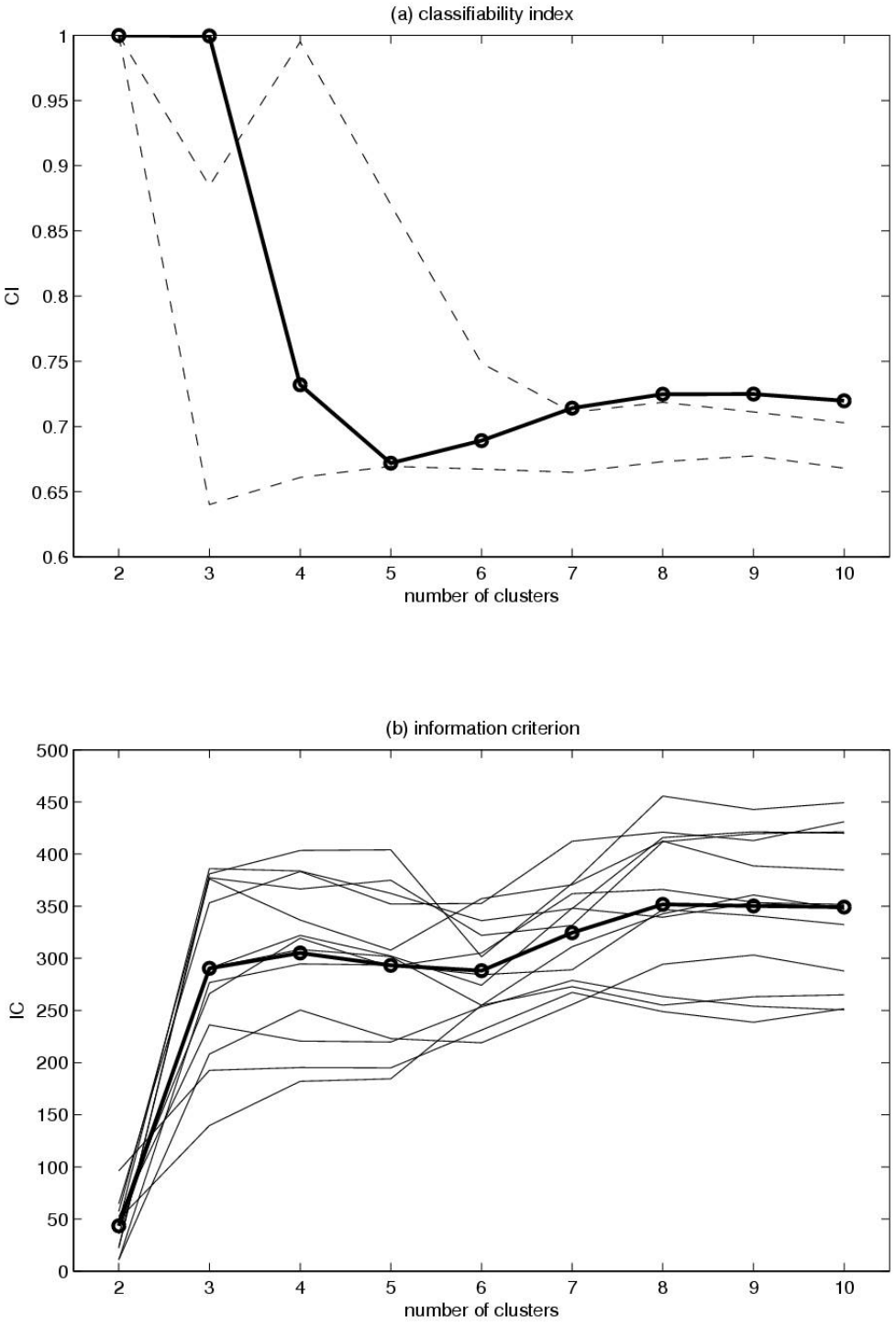

Figure 3: (a) Classifiability Index – CI – (Michelangeli *et al.*, 1995) for 2-10 clusters (bold line with circle) defined with *k*-means on the 7 leading principal components (PCs) of zonal and meridional components of ERA-40 winds at 925, 700 and 200 hPa. The dashed line give the CI two-sided 90% confidence interval extracted from 100 simulations with red noise having the same covariance at lag 0 and 1 as the 7 leading PCs of wind data. (b) Information Criterion (Santos *et al.*, 2005) computed on daily rainfall with a threshold of 1 mm. Each station is displayed as a thin line while the bold line with dots represents the country average. The 2-10 clusters are defined with k-means on the 7 leading principal components of zonal and meridional components of ERA-40 winds at 925, 700 and 200 hPa.

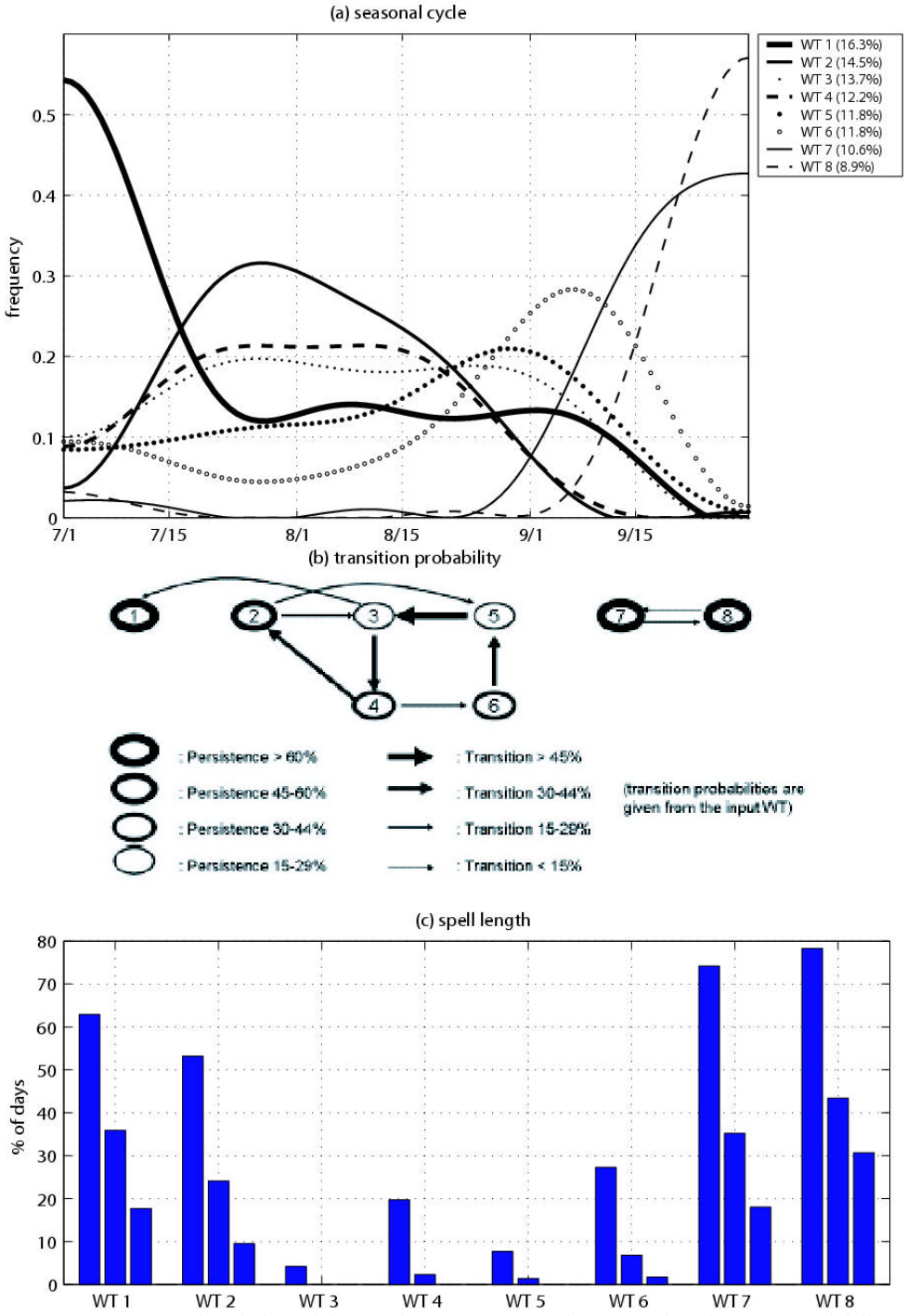

Figure 4: (a) Seasonal variation of the weather types (WT). The seasonal cycle (= mean of daily value) is smoothed by a low-pass filter retaining periods lower than 1/30 cycle-per-day; (b) probability transition between the weather types The arrows indicate the transition that occurs more likely than chance at the one-sided 99% level (Vautard *et al.*, 1990) and the circles around the weather types is proportional to the one-day persistence (i.e. the probability that a WT on day *d* is the same on day *d*+1); (c) % of days of each types included in homogenous spells lasting at least 3, 5 and 7 days.

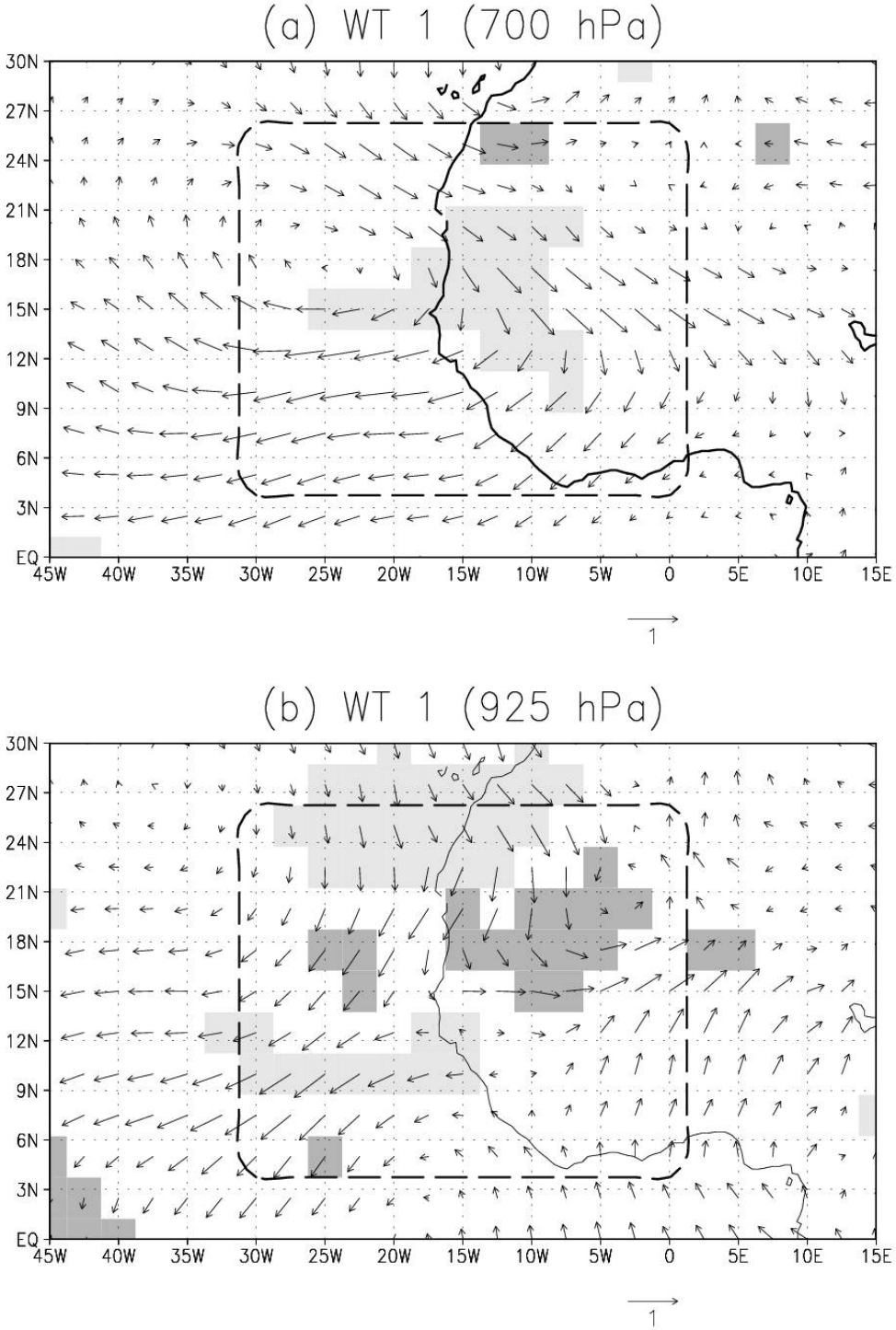

Figure 5: Composite maps of (a) 700 hPa, and (b) 925 hPa anomaly winds of weather type (WT) 1. The raw data from July, 1961 to September 30, 1998 are normalized to zero mean and unit variance before the computation of the composite. Shading indicates composite anomalies of divergence greater than 0.25 (light) and less than –0.25 (dark). Divergence (*D*) is computed from the raw zonal (*u*) and meridional (*v*) winds in Cartesian coordinates ($D = \frac{du}{dx} + \frac{dv}{dy}$) and then standardized to zero mean and unit variance. Positive (negative) values indicate anomalous divergence (convergence). The weather types are computed from wind data in 30°W-0°; 2.5°-27.5°N delineated by a dashed black box.

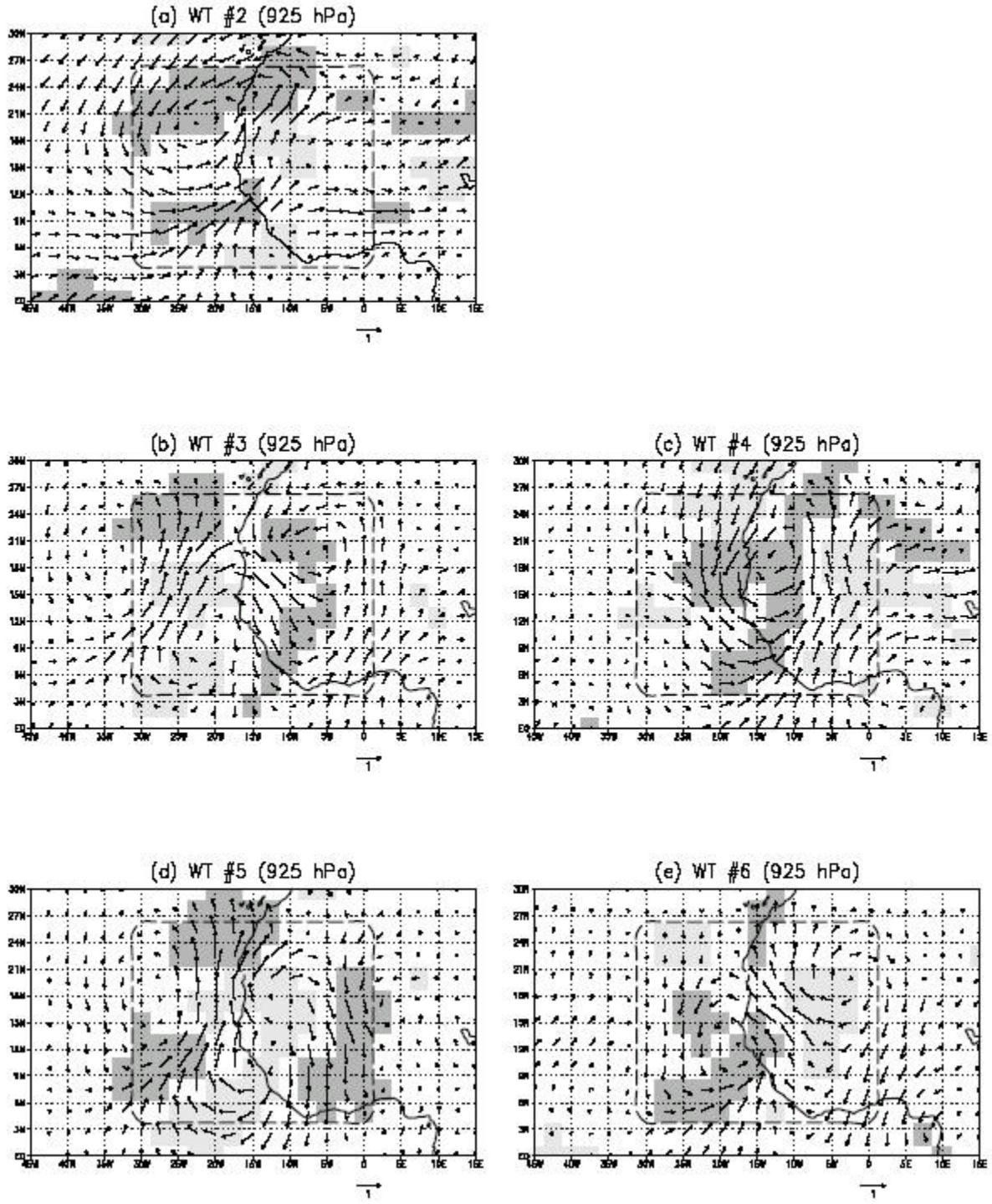

Figure 6: Composite maps of 925 hPa anomaly winds for (a) weather type (WT) 2, (b) WT3, (c) WT4 (d), WT5 and (e) WT6. Shading indicates composite anomalies of divergence greater than 0.25 (light) and less than –0.25 (dark). Details as in Fig. 5.

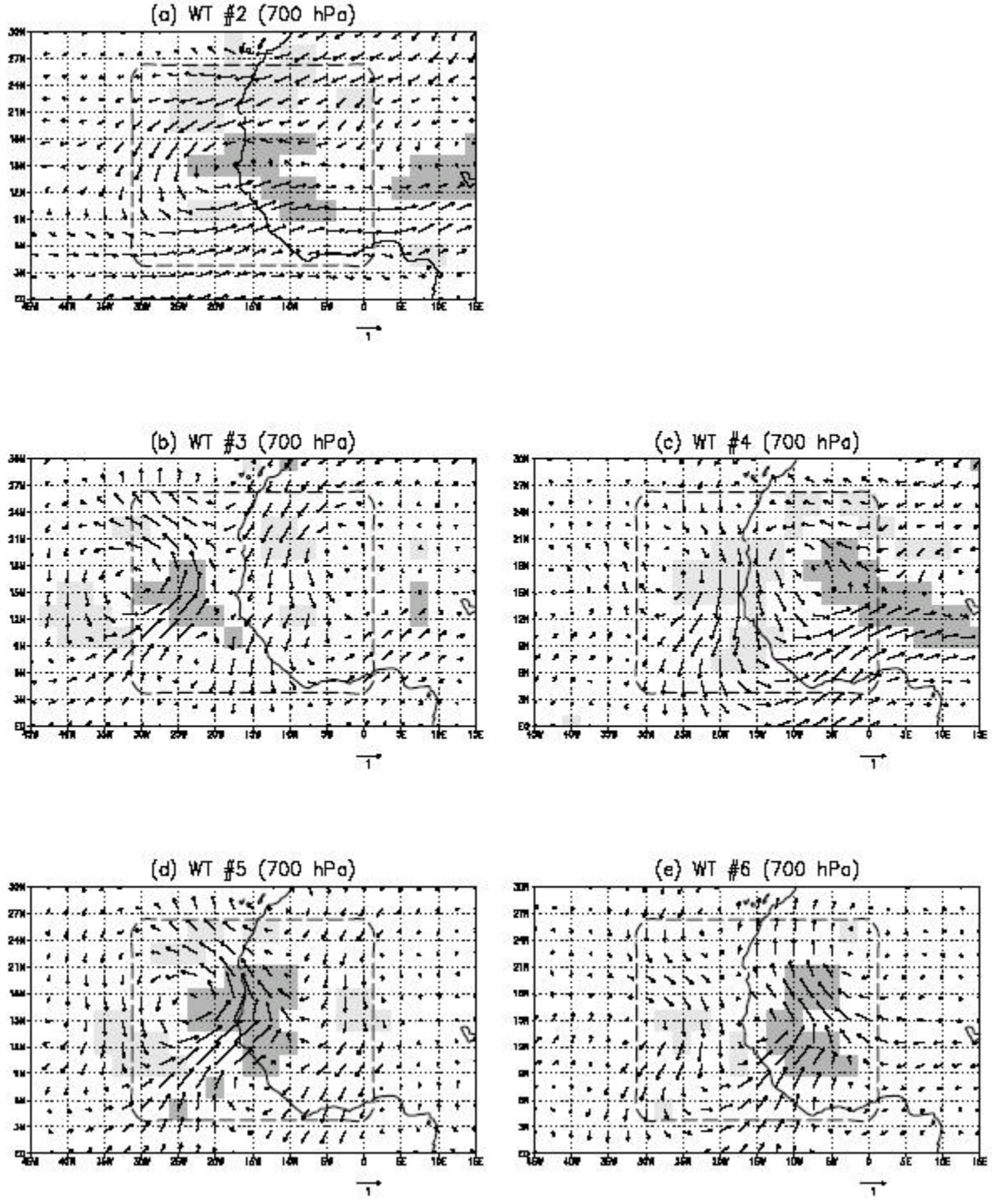

Figure 7: Same as Fig. 6 for 700 hPa anomaly winds.

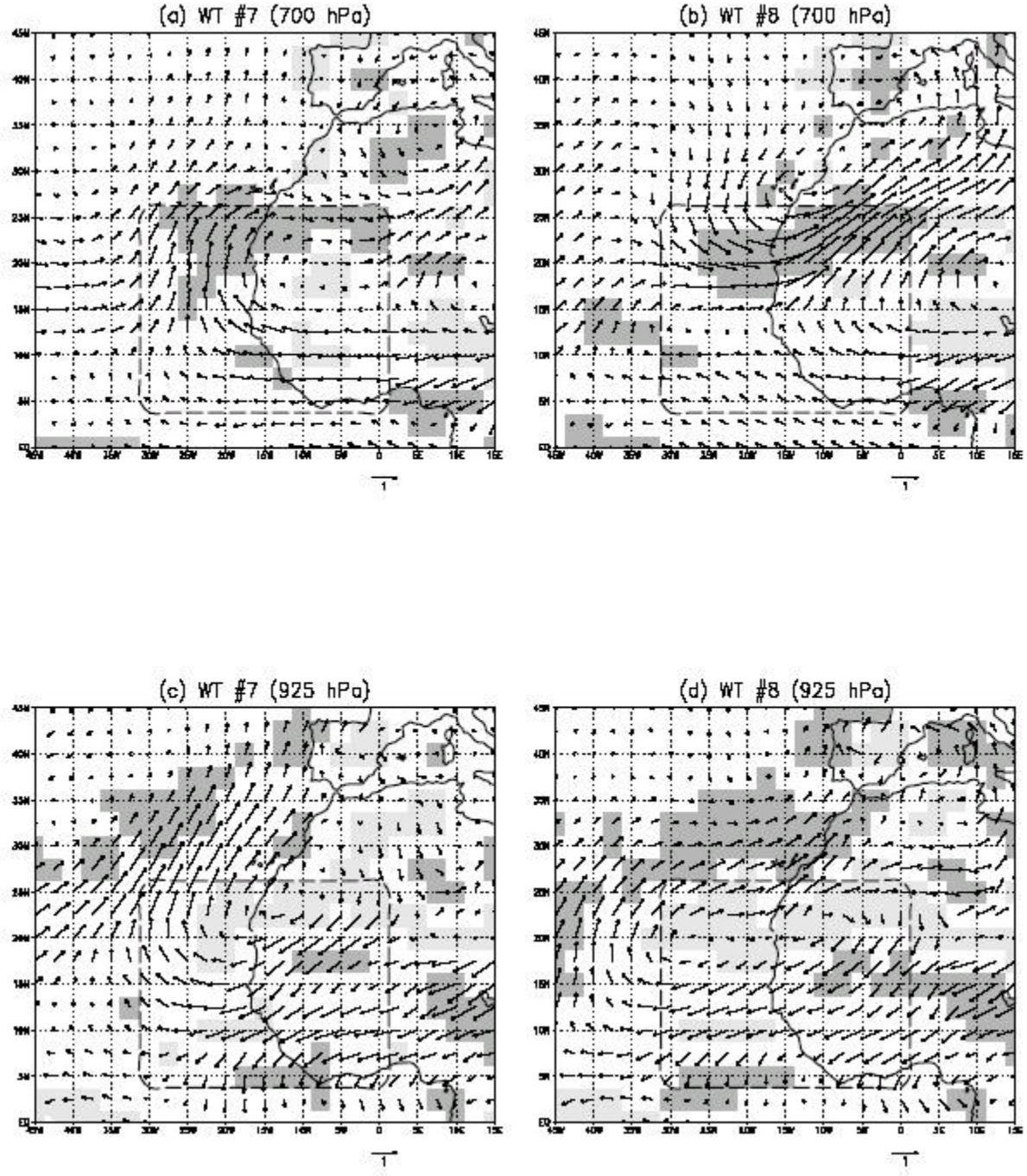

Figure 8: Composite maps of anomaly winds and divergence for weather types (WT) 7 and 8: (a) 700 hPa for WT7, (b) 700 hPa for WT8, (c) 925 hPa for WT7, (d) 925 hPa for WT8. Details as in Fig. 5.

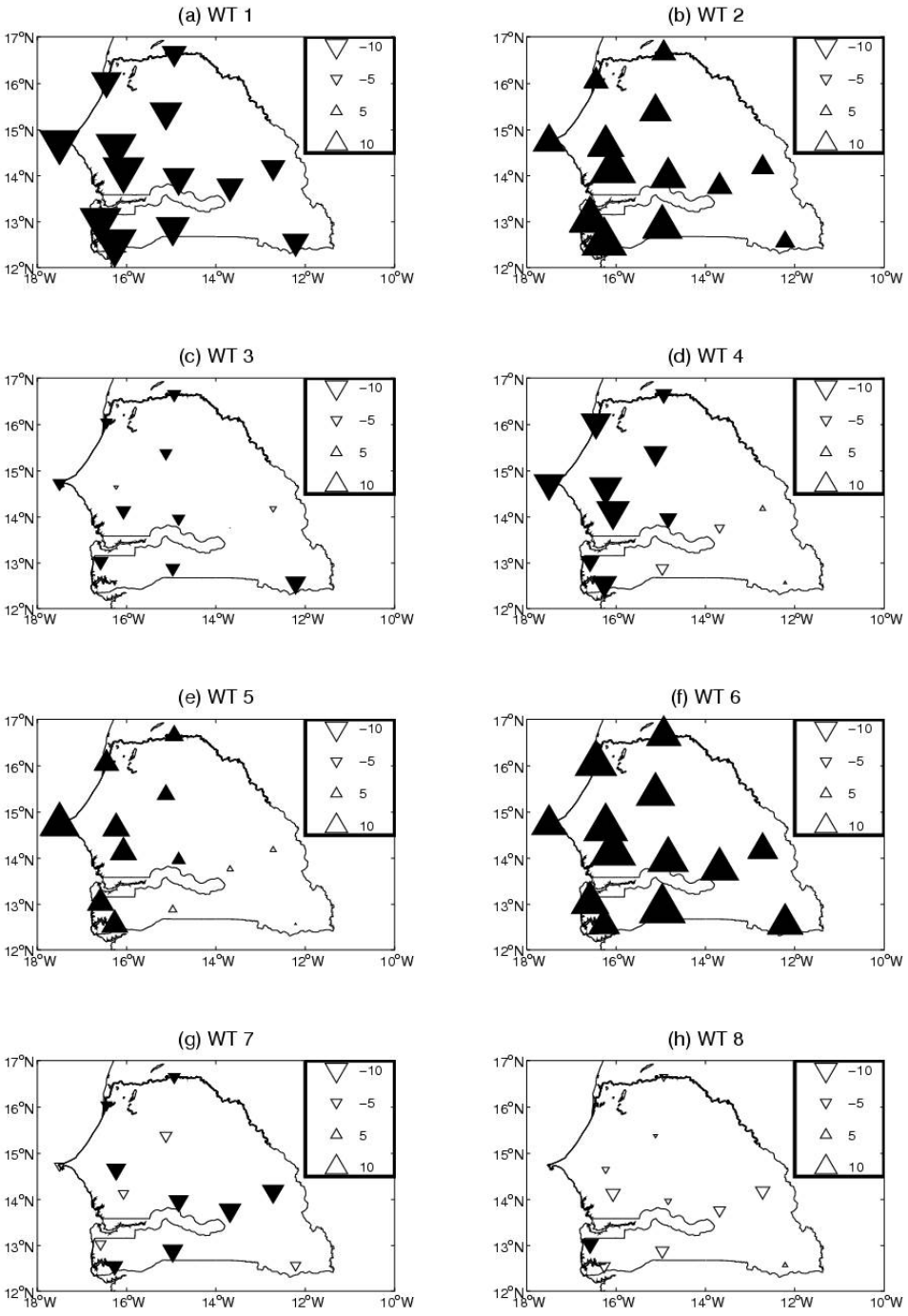

Figure 9: Rainfall occurrence anomalies (in %) associated for (a) weather type (WT) 1, (b) WT2, (c) WT3, (d) WT4, (e) WT5, (f) WT6, (g) WT7, (h) WT8. Significant values at the one-sided 99% level according to a chi-square test (null hypothesis is that the probability of rainfall > 1 mm during the days belonging to a given WT is the same as the one of the remaining days) are filled in black.

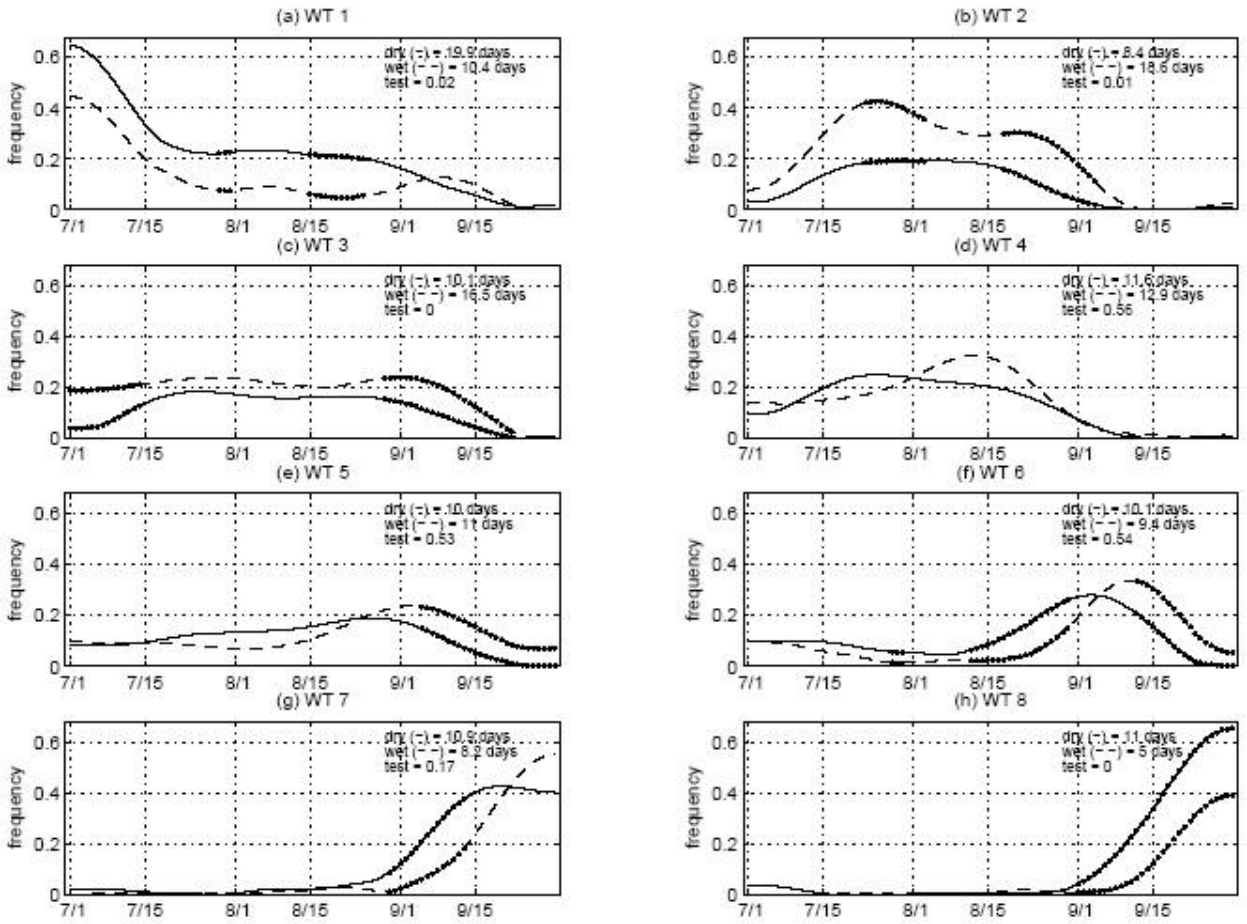

Figure 10: Mean seasonal cycle of weather type (WT) frequency for the 10 driest (full line) and 10 wettest (dashed line) July-September seasons. The selected seasons are determined from the standardized anomaly index of rainfall occurrence (see text). The WT frequency was computed on a daily basis from each sample of 10 years, and then smoothed for clarity using a recursive low-pass filter retaining only frequencies lower than 1/30 cycle-per-day. A dot on each curve indicates a significant difference between both samples at the two-sided 95% level according to a Student's T test (the null hypothesis is that the mean frequency of both samples is equal). The mean occurrence frequency for each WT during the 10 driest and 10 wettest seasons are indicated (in days per July-September season) in the upper right corner of each panel, along with the Student's T Test p-value of the difference between dry and wet samples.

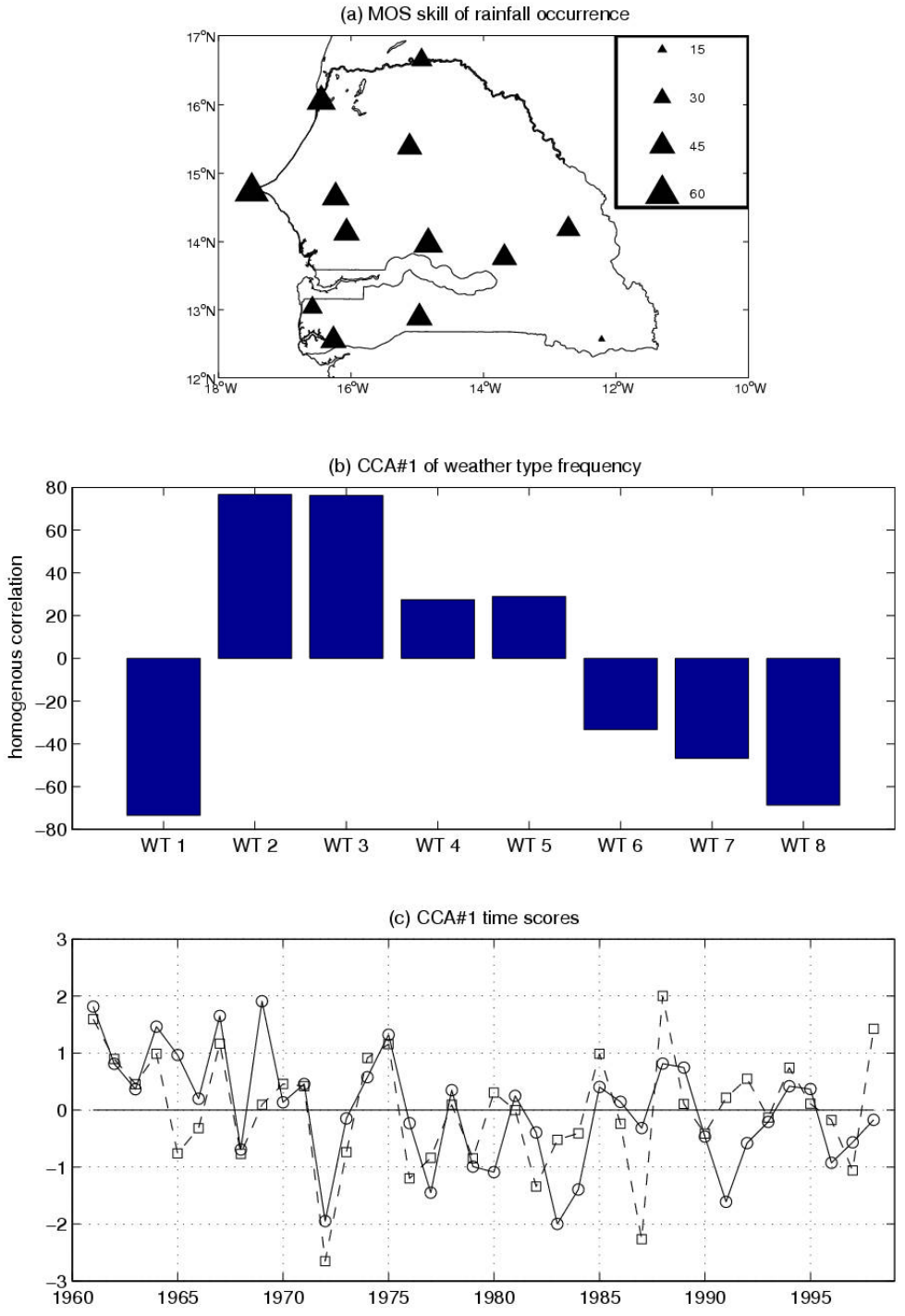

Figure 11: Leading mode of a cross-validated CCA between interannual anomalies of weather type frequency and station rainfall frequency ; (a) correlations x 100 between the observed and "predicted" rainfall frequency ; (b) homogeneous correlation of weather type frequency ; (c) CCA time series of weather type frequency (dashed line and square) and station rainfall frequency (solid line and circle) in standardized values. The homogenous correlations in (b) are the correlations between weather type frequency and the cross-validated time series associated with its CCA pattern (dashed line in panel c).

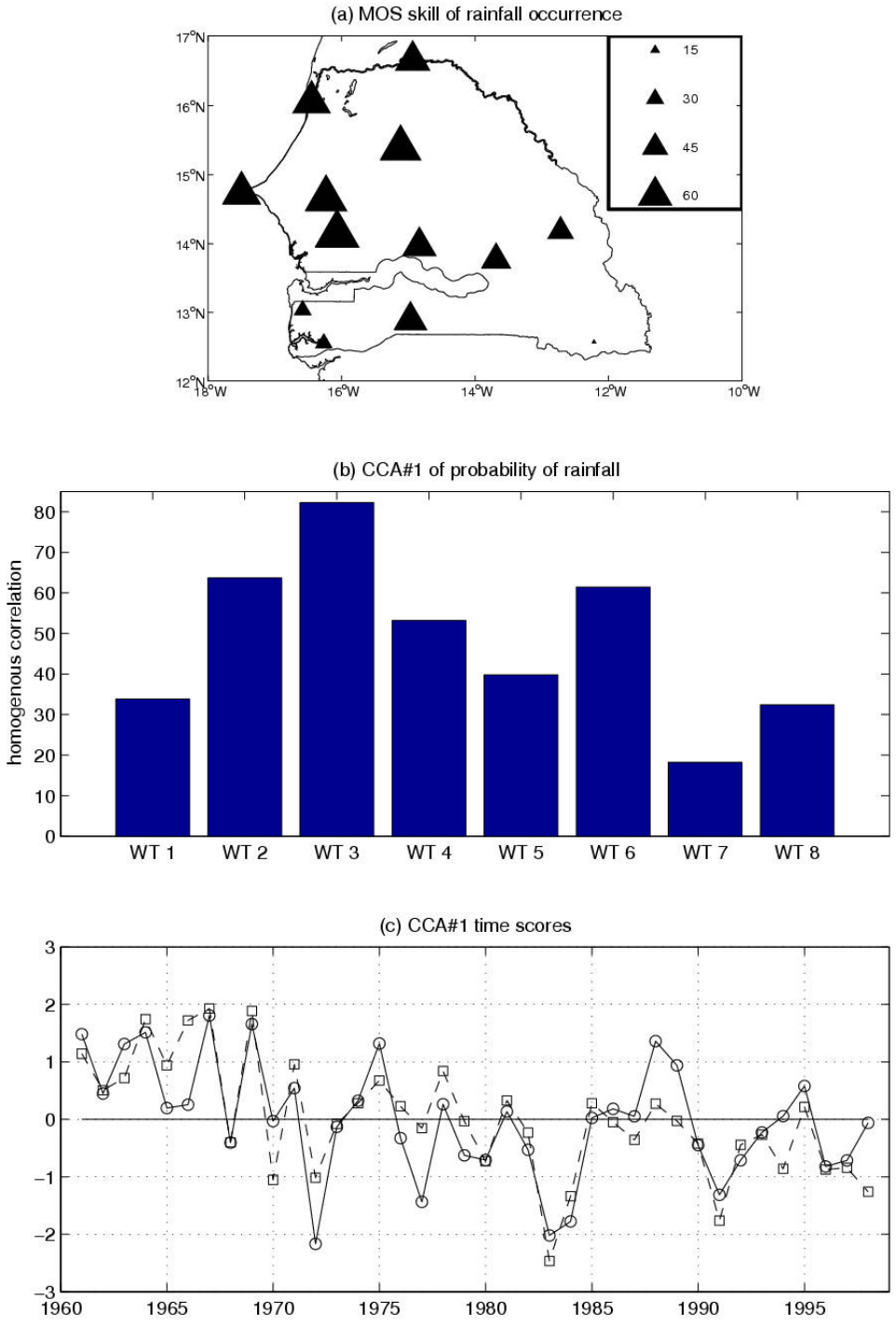

Figure 12: Leading mode of a cross-validated CCA between interannual anomalies of the average rainfall probability within each weather type and station rainfall frequency; (a) correlations between the observed and "predicted" rainfall frequency ; (b) homogeneous correlation of weather type average rainfall probability; (c) CCA time series of weather type average rainfall probability (dashed line and square) and frequency of occurrence of rainfall (solid line and circle) in standardized values. The homogenous correlations in (b) are the correlations between rainfall probability within each weather type and the cross-validated time series associated with its CCA pattern (dashed line in panel c).

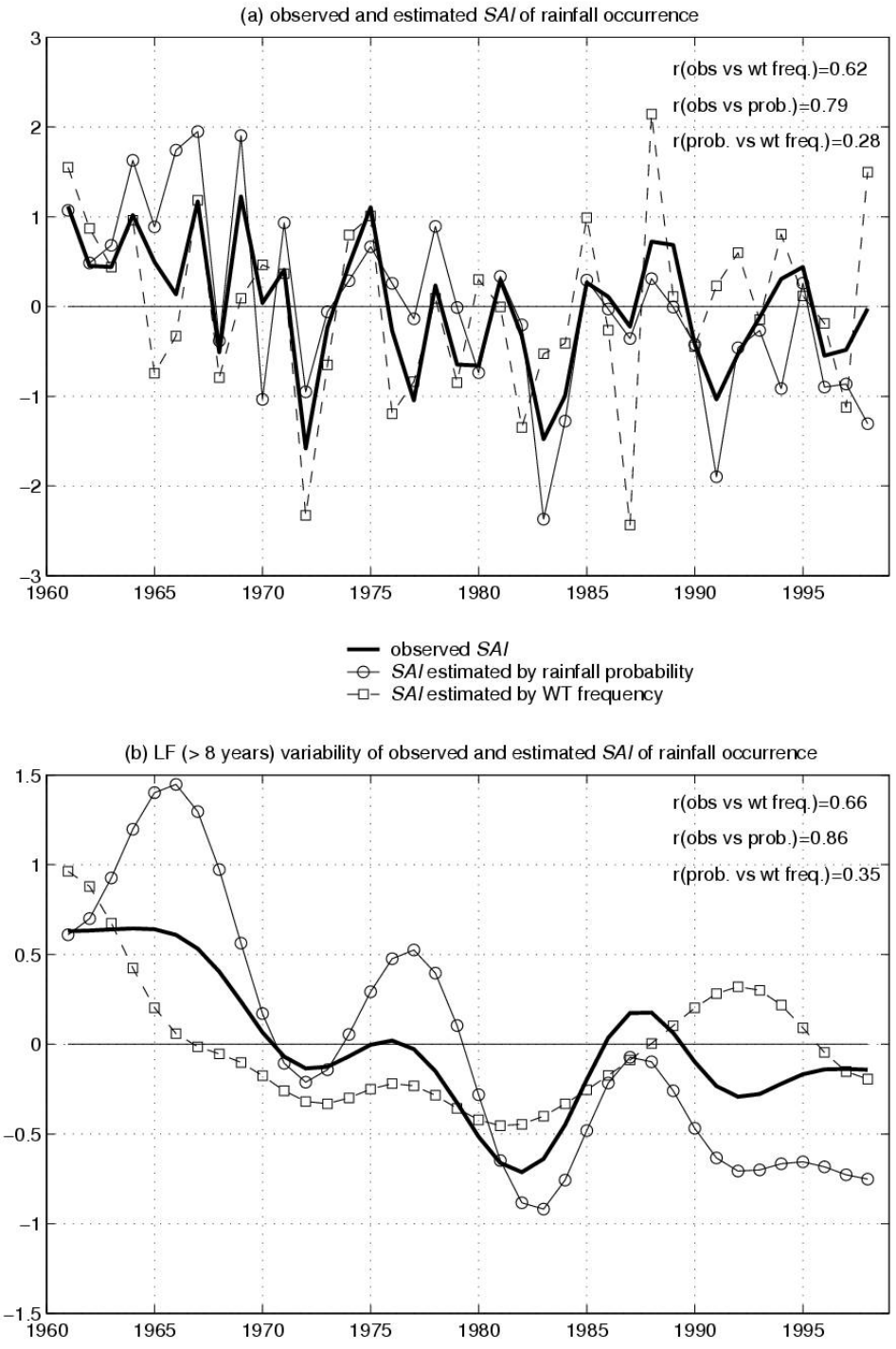

Figure 13: (a) Standardized anomaly index (*SAI*) of observed rainfall frequency (thick line), estimated rainfall frequency hindcast by the CCA between rainfall frequency and average probability of rainfall occurrence of each weather type (full line + circle), and by the CCA between rainfall frequency and weather type frequency (dotted line + square). (b) Same as (a) for the low-frequency component. The low-frequency is extracted by a recursive low-pass filter removing high frequencies higher than 1/8 cycle-per-year.

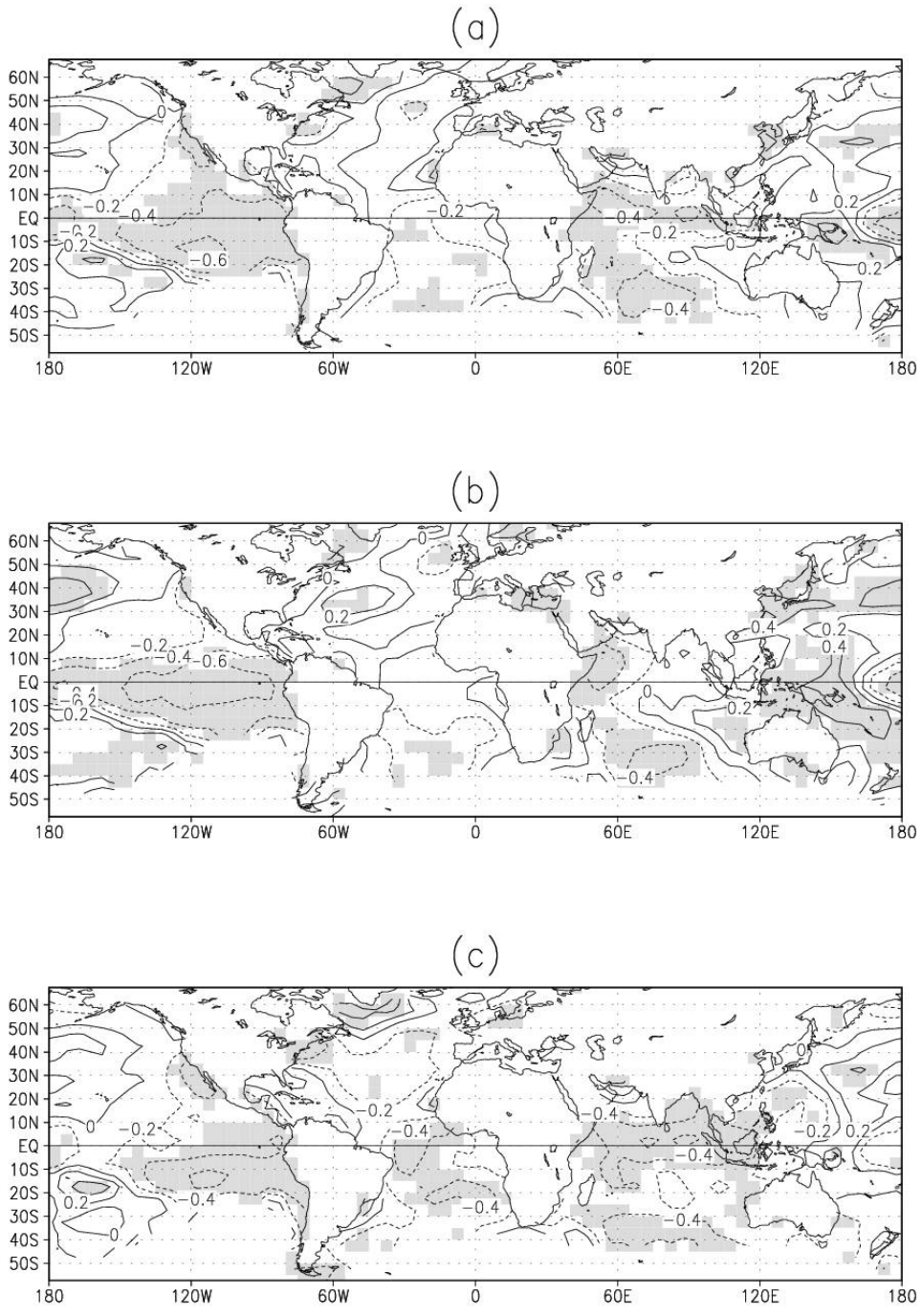

Figure 14: Correlation between observed SST in July-September and (a) observed standardized anomaly index (*SAI*) (from rainfall occurrence > 1 mm), (b) leading CCA mode of the weather type frequency (dashed line with squares in Fig. 11c) and (c) leading CCA mode of the average probability of rainfall of each weather type (dashed line with squares in Fig. 12c). The contours are indicated at -0.6, -0.4, -0.2, 0, 0.2, 0.4, 0.6 and shadings indicate local significant correlations at the two-sided 95% level according to a random-phase test (Janicot *et al.*, 1996; Ebisuzaki, 1997).